A mutually induced conformational fit underlies Ca^{2+}-directed interactions between calmodulin and the proximal C terminus of KCNQ4 K^+ channels

Received for publication, November 26, 2018, and in revised form, February 24, 2019 Published, Papers in Press, February 26, 2019, DOI 10.1074/jbc.RA118.006857

Crystal R. Archer[‡§], Benjamin T. Enslow[¶], Alexander B. Taylor[§], Victor De la Rosa[‡1], Akash Bhattacharya[§2], and Mark S. Shapiro[‡3]

From the Departments of [‡]Cell and Integrative Physiology and [§]Biochemistry and Structural Biology and the [¶]Long School of Medicine, University of Texas Health San Antonio, San Antonio, Texas 78229

Edited by Roger J. Colbran

Calmodulin (CaM) conveys intracellular Ca^{2+} signals to KCNQ (Kv7, "M-type") K^+ channels and many other ion channels. Whether this "calmodulation" involves a dramatic structural rearrangement or only slight perturbations of the CaM/KCNQ complex is as yet unclear. A consensus structural model of conformational shifts occurring between low nanomolar and physiologically high intracellular [Ca^{2+}] is still under debate. Here, we used various techniques of biophysical chemical analyses to investigate the interactions between CaM and synthetic peptides corresponding to the A and B domains of the KCNQ4 subtype. We found that in the absence of CaM, the peptides are disordered, whereas Ca^{2+}/CaM imposed helical structure on both KCNQ A and B domains. Isothermal titration calorimetry revealed that Ca^{2+}/CaM has higher affinity for the B domain than for the A domain of KCNQ2–4 and much higher affinity for the B domain when prebound with the A domain. X-ray crystallography confirmed that these discrete peptides spontaneously form a complex with Ca^{2+}/CaM, similar to previous reports of CaM binding KCNQ-AB domains that are linked together. Microscale thermophoresis and heteronuclear single-quantum coherence NMR spectroscopy indicated the C-lobe of Ca^{2+}-free CaM to interact with the KCNQ4 B domain (K_d ~10–20 μM), with increasing Ca^{2+} molar ratios shifting the CaM-B domain interactions via only the CaM C-lobe to also include the N-lobe. Our findings suggest that in response to increased Ca^{2+}, CaM undergoes lobe switching that imposes a dramatic mutually induced conformational fit to both the proximal C terminus of KCNQ4 channels and CaM, likely underlying Ca^{2+}-dependent regulation of KCNQ gating.

Calmodulin (CaM)[4] is a highly conserved Ca^{2+} sensor among vertebrates involved in a variety of physiological roles, with at least 300 known binding targets (1, 2). The N and C termini of CaM form globular clusters called the N-lobe and C-lobe, respectively, which are connected by a flexible linker. Two Ca^{2+}-binding sites localize to each lobe via "EF-hand" motifs with the N-lobe containing EF-I and -II, and the C-lobe EF-III and -IV (3). For free CaM protein (*i.e.* CaM not bound to a target protein), the estimated affinity of Ca^{2+} for the N-lobe is K_d ~10 μM, and for the C-lobe it is K_d ~1 μM, affinities that often change when CaM is bound to target proteins (4–6). In neurons and other cells, in which global resting (tonic) $[Ca^{2+}]_i$ is estimated to be 30–150 nM (7, 8), non-Ca^{2+}-loaded CaM (apoCaM) is thought to exist in its "off state." During physiological cytoplasmic increases of $[Ca^{2+}]_i$ up to ~5 μM globally and ~100 μM in localized nanodomains (9), CaM transitions to an "on-state" that modifies the function of bound target proteins. Solution NMR studies indicate that free apoCaM adopts a semi-closed conformation, in which the N- and C-lobes are usually folded toward each other (10). Upon Ca^{2+} loading, the lobes extend in an open conformation, exposing distinct motifs that often direct CaM to wrap around its target proteins to initiate signaling cascades and regulate physiological function in response to Ca^{2+} signals (11).

This work was supported by National Institutes of Health Grants R01 NS 043394 and NS 094461 (to M. S. S.), a Faculty Scholar Award (to M. S. S.), a grant from the Morrison Trust Foundation (to M. S. S.), NINDS/National Institutes of Health NRSA predoctoral training fellowship F31 NS090887 (to C. R. A.), National Institutes of Health/NHLBI postdoctoral training grant T32 HL007446 (to C. R. A.) (directed by James D. Stockand), NIH Grant R01 AI104476 (to Dmitri Ivanov supporting A. B.) and a core usage support grant from the IIMS CTSA at UT Health San Antonio (Department of Medicine). Part of this work was performed at the Northeastern Collaborative Access Team beamlines, which are funded by a program project grant from the NIGMS/NIH (P30 GM124165). The Eiger 16M detector on the 24-ID-E beam line is funded by NIH-ORIP HEI Grant S10-OD021527. This research used resources of the Advanced Photon Source, a user facility operated for the DOE, Argonne National Laboratory under Contract DE-AC02–06CH11357. The authors declare that they have no conflicts of interest with the contents of this article. The content is solely the responsibility of the authors and does not necessarily represent the official views of the National Institutes of Health.

This article contains Table S1 and Figs. S1–S6.

The atomic coordinates and structure factors (code 6N5W) have been deposited in the Protein Data Bank (http://wwpdb.org/).

[1] Present address: CONACYT, Facultad de Medicina, Universidad Autónoma de San Luis Potosí 78210, México.

[2] Present address: Beckman Coulter Life Sciences, 5600 Lindbergh Dr., Loveland, CO 80538.

[3] To whom correspondence should be addressed: Dept. of Cell and Integrative Physiology, University of Texas Health at San Antonio, STRF, MC 8253, 8403 Floyd Curl Dr., San Antonio, TX 78229. Tel.: 210-562-4092; Fax: 210-562-4060; E-mail: shapirom@uthscsa.edu.

[4] The abbreviations used are: CaM, calmodulin; HSQC, heteronuclear single-quantum coherence; TROSY, transverse relaxation optimized spectroscopy; MΩ, megaohms; apoCaM, non-Ca^{2+}-loaded CaM; VGCC, voltage-gated Ca^{2+} channel; RD, regulatory domain; PIP_2, phosphatidylinositol 4,5-bisposphate; PDB, Protein Data Bank; HBS, Hepes-buffered saline; RMSD, root mean square deviation; ITC, isothermal titration calorimetry; MST, microscale thermophoresis; CHO, Chinese hamster ovary; LB, Luria broth.

Since the unexpected revelation that the well-known Ca^{2+} sensitivity of voltage-gated Ca^{2+} channels (VGCCs) and SK-type Ca^{2+}-activated K^+ channels are due to direct interactions with CaM, without the need for any kinases (12–14), a number of other channels have been shown to be similarly regulated by Ca^{2+} ions (15). Particularly studied for CaM actions on VGCCs is the issue of apoCaM pre-association with the channels and the complex dynamic changes of the configuration of CaM between metal-free and Ca^{2+}-loaded states. These changing configurations often involve "lobe switching" and have proved surprisingly distinct between the Ca_V1 (L-type) and Ca_V2 (N- and P/Q-type) channels (16–22). For SK channels, similar issues are being studied, stemming from the surprising early conclusion that the high-affinity C-lobe of CaM is involved in pre-association with the channels (with neither EF-hand in the C-lobe occupied by Ca^{2+} and the lower-affinity N-lobe acting as the Ca^{2+} sensor, or "Ca^{2+} switch," for gating). Consistent with that earlier structural hypothesis (12, 23–25) is a recent cryo-EM structure of a Ca^{2+}/CaM-bound SK4 channel (26).

In neurons, heart, and smooth muscle, tetrameric voltage-gated KCNQ (Kv7, "M-type") K^+ channels play critical roles in regulating cellular excitability (27). CaM has been shown to regulate the trafficking and expression of KCNQ channels as well as their gating (28–31). CaM acts as the Ca^{2+} sensor for KCNQ channels via direct interactions with the proximal C terminus, thereby mediating the Ca^{2+}-dependent modulatory action of several types of receptors linked to phospholipase C (7, 30, 32, 33). It has been presumed for KCNQ channels that Ca^{2+} loading of certain EF-hands of CaM induces a conformational change that inhibits channel opening. For KCNQ1-containing channels, however, Ca^{2+} loading of CaM augments opening (34), perhaps in accord with their role in cardiomyocytes, inner ear, and epithelia in which KCNQ1 almost always is expressed together with KCNE β-subunits (35, 36). In all cases, the extent and manner of pre-association of apoCaM with the channels and the nature of that conformational change are vigorously under debate.

It has been argued that apoCaM is required for KCNQ channels to properly function (28, 31, 34, 37–39), but it is still unclear whether truly metal-free CaM pre-associates with the channels. All studies have shown two highly conserved domains in the proximal C terminus, the A and B domains, as the loci of CaM actions (Fig. 1, *A* and *B*). This proximal half of the C terminus, which we call the regulatory domain (RD), besides containing highly conserved A and B domains involved in CaM interactions (39, 40), also contains sites of regulation of opening by phosphatidylinositol 4,5-bisphosphate (PIP_2) (41) and protein kinase C, the regulatory site of the latter being just after the B domain (42–44). Rich interplay between these molecules at the RD is proposed to exquisitely regulate KCNQ channels.

Recent structural investigations suggest either that Ca^{2+}/CaM embraces both the A and B domains of KCNQ1, -4, and -5 and KCNQ2/3 hybrids (45–47) or that Ca^{2+}-loading of CaM induces the A domain to be released from the trimeric complex, leaving Ca^{2+}-loaded CaM to wrap tightly around the B domain alone (48, 49). In contrast, a recent solution NMR study of a similar complex of the A and B domains of KCNQ2 and CaM suggested only minor changes in the structure of the complex between low and high [Ca^{2+}], arguing against a dramatic structural change in KCNQ channels in response to intracellular rises in [Ca^{2+}] (50).

We investigated this issue for KCNQ4, as this isoform is expressed in cells and tissues mainly as homomeric channels, simplifying our interpretations. We used a gamut of biophysical chemical and structural analyses, such as heteronuclear single-quantum coherence NMR spectroscopy (HSQC-NMR) and X-ray crystallography. In our investigations, we used separate synthetic peptides corresponding to the A and B domains of KCNQ2–4 to gain better insight into CaM interactions with the domains independent from each other. We were scrupulously careful to know both the free [Ca^{2+}] and the stoichiometric ratios of [Ca^{2+}], CaM, and A and/or B domains in all of our experiments. The goal of this inquiry was to build a stepwise model of the mechanism of CaM binding to the KCNQ4 C terminus from $<$10 nM to physiologically high [Ca^{2+}].

Results

The A and B domains appear intrinsically disordered in the absence of CaM

The amino acid sequences of the A and B domains of KCNQ channels are conserved within the KCNQ family (Fig. 1*B*). The A domain, also known as the "A helix," contains a highly conserved IQ*XX*R amino acid sequence characteristic of IQ CaM-binding motifs found in a multitude of other CaM target proteins (51). The A domain also contains 1–12 and 1–16 motifs. The B domain, also called the "B helix," contains multiple canonical and noncanonical CaM-binding motifs, including 1-5-10 and 1–14 hydrophobic anchoring residues (52). Having multiple CaM motifs within the RD suggests that CaM may adopt several different orientations when binding to KCNQ channels, as recently suggested (50).

The existing co-crystal and cryo-EM structures of CaM with purified full channel and purified fragments containing the A and/or B domains show the A and B domains adopting an α-helix secondary structure or assembled in coiled-coil arrangements when embraced by CaM (45–47, 49). However, it is not known whether the free A and B domains of KCNQ channels adopt helical structure in the absence of CaM, despite their common reference as the "A helix" or "B helix." We used CD spectroscopy to analyze the secondary structure of synthesized peptides corresponding to the A or B domains of KCNQ2–4 subunits. Although peptides typically appear disordered in the absence of a binding partner, CD can indicate whether they adopt secondary structure on their own, such as that corresponding to the NSCate domain of L-type Ca^{2+} channels, which has α-helical structure in the absence of CaM (53). Each of the KCNQ peptides displayed single peaks at 205 or 220 nm (Fig. 1*C*), suggesting that the A and B domains may be intrinsically disordered in the absence of CaM and require CaM to adopt their coiled-coil nature in reported structures. In contrast, CaM displayed dual peaks at 208 and 222 nm, which is the signature for proteins with α-helices. Because the CD buffer contained Ca^{2+} in equimolar ratio to protein, the CaM in this experiment is expected to only be partially Ca^{2+}-bound. This

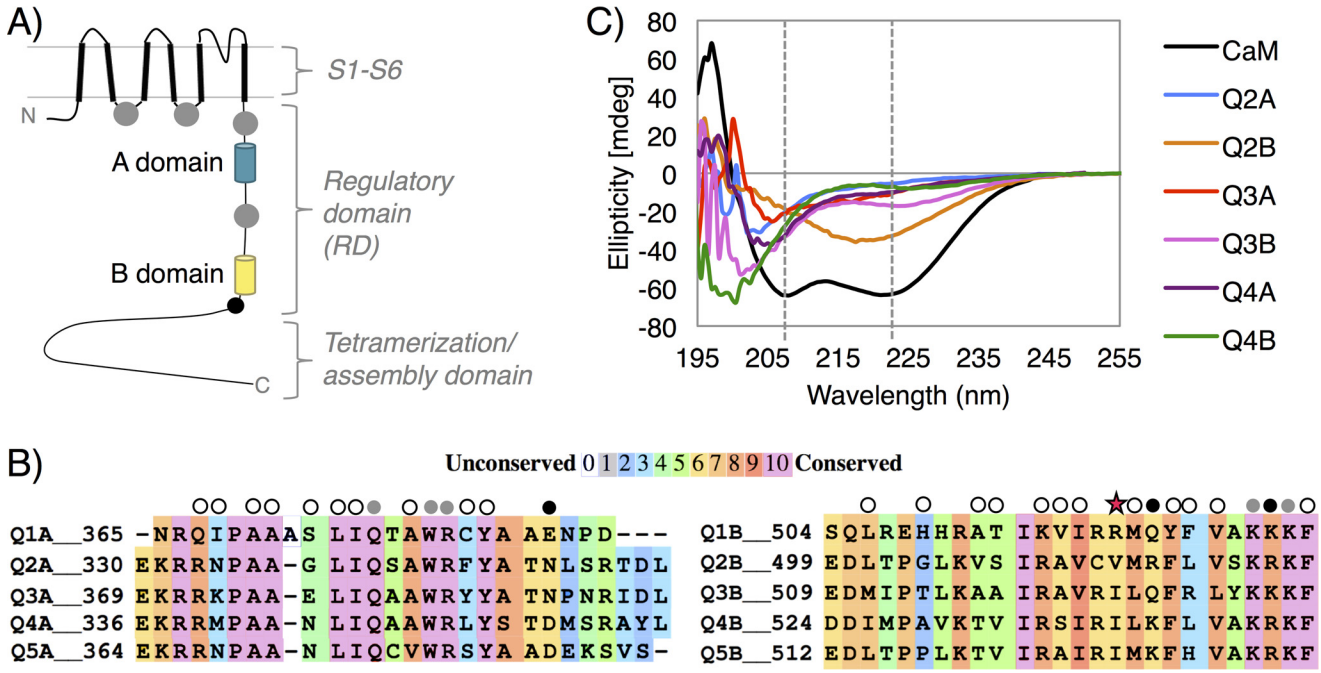

Figure 1. KCNQ1–5 contain conserved A and B domains, which are disordered in the absence of CaM. *A*, representative *schematic* of a KCNQ protein subunit depicting the S1–S6 transmembrane helices, the intracellular N and C termini, and the A domain (*teal*) and B domain (*gold*) within the proximal half of the C terminus, referred to as the RD. The schematic does not show the likely intimate proximity of the RD to the plasma membrane. For reference, the PIP_2 interaction sites are shown as *gray circles*, and the protein kinase C phosphorylation site conserved between KCNQ2–5 is represented by a *black circle*. *B*, sequence alignments of the A domain (*left*) and B domain (*right*) of human KCNQ1–5 subunits taken from Uniprot. All sequences represent "isoform 1" of each subunit, with the exception of the KCNQ2 sequences that represent the universally used isoform 4 and those of KCNQ4a. Alignments were performed using the PRALINE alignment tool, and the *colors* were adjusted using Photoshop Elements. The *dots above* the alignments indicate the interactions with Ca^{2+}/CaM shown in Fig. S3 and Fig. 2. *Black dots* indicate the residues with strong interactions between the KCNQ4 peptides and CaM that are different from those of KCNQ1, and *gray dots* indicate strong interactions for which the interacting residues are conserved. *Open circles* indicate those KCNQ4 residues having nonbonded contacts with CaM, and the *star* indicates the residues of KCNQ1 that may cause changes of the CaM backbone compared with KCNQ4. *C*, CD spectra of the peptides used in this study and of CaM. *Two dashed vertical lines* at 208 and 222 nm indicate the points of deflection typical of proteins such as CaM (*black*) with high helical content. All of the Q2-4 A and B peptides appear to lack helical content in the absence of CaM.

experiment also suggests that Ca^{2+} does not directly induce the secondary structure of the A and B domains. To highlight the malleable nature of these CaM-binding domains, we generally call these regions the "A and B domains" in this study. Under "Discussion," we comment on the importance of these observations in the role of CaM in proper channel expression.

The independent Q4A and Q4B peptides adopt an anti-parallel α-helical conformation enveloped by CaM in the presence of Ca^{2+}

To determine with high resolution how CaM and the independent A and B domains of KCNQ4 spontaneously assemble under conditions of high [Ca^{2+}], compared with existing structures of CaM that have been *co*-expressed with proteins of the connected KCNQ-AB fragments, we obtained the X-ray crystal structure of Ca^{2+}/CaM in complex with KCNQ4 A domain (Q4A) and KCNQ4 B domain (Q4B) peptides. We refer to this structure as Ca^{2+}/CaM:Q4A:Q4B (PDB entry 6N5W) (Fig. 2*A*). Elongated, hexameric crystals grew to full size after 8 days at room temperature in the presence of 2 mM free [Ca^{2+}]. No crystals were observed in Ca^{2+}-free conditions (in a formation buffer of HBS plus 2 mM EGTA) in our extensive array of crystallization screens. The X-ray structure of Ca^{2+}/CaM:Q4A:Q4B was determined by molecular replacement using the structure of Ca^{2+}/CaM:KCNQ1-AB (PDB entry 4UMO) as a model and refined to a resolution of 2.15 Å (crystallographic statistics found in Table S1). The trimeric structure includes residues 4–147 of CaM, Arg^{338}–Asp^{356} of Q4A, and Asp^{525}–Phe^{549} of Q4B. The schematic in Fig. 2*B* illustrates our understanding of this complex as it exists within the entire KCNQ4 subunit. A common observation of existing structures of Ca^{2+}/CaM with the A and B domains of KCNQ1 and KCNQ4 and of the frog oocyte KCNQXem channel is that Ca^{2+} is shown coordinated by both EF-hands in the N-lobe but is only occasionally present in EF-hands of the C-lobe. This has been a surprising finding, because, as mentioned above, for free CaM in isolation, the EF-hands in the C-lobe have a higher affinity for Ca^{2+} than does the N-lobe, although this discrepancy was also seen previously for VGCCs and SK channels (54). Our Ca^{2+}/CaM:Q4A:Q4B crystal structure also shows EF-hands I and II of the CaM N-lobe to each coordinate a Ca^{2+} ion. EF-III and -IV are empty, despite this complex being formed in a buffer containing an excess of Ca^{2+} (albeit modest) relative to the number of EF-hands (222 μM CaM and 2 mM Ca^{2+}). The crystallization buffer contained citrate, which also binds Ca^{2+} but with much lower affinity than CaM ($K_a = 10^{3.5}$ M^{-1}) (55). Citrate has also been shown to directly interact with the C-lobe of CaM, but we do not observe such an interaction in this structure (56). We also point out that the Ca^{2+}/CaM:Q1AB structure was not obtained in a high-citrate buffer (48) but is very similar to this structure (RMSD = 1.68 Å) and was also found to lack Ca^{2+} ion density in

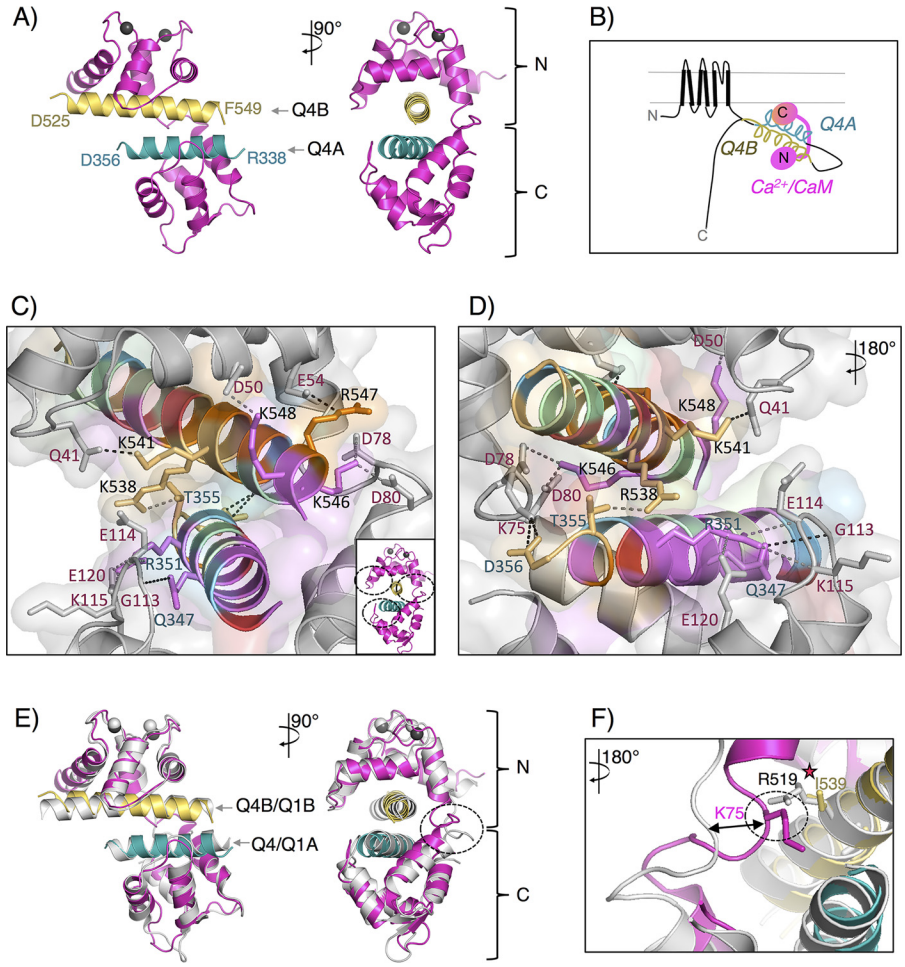

Figure 2. The X-ray crystal structure of the Ca^{2+}/CaM:Q4A:Q4B complex involves antiparallel A and B helices enveloped by CaM with Ca^{2+} ions in the N-lobe. *A*, *front view* (*left*) and 90° *side view* (*right*) of the trimeric co-crystal X-ray structure of Ca^{2+}/CaM with the Q4A and Q4B peptides. CaM is shown in *pink*, with the C-lobe facing the *bottom*, lacking Ca^{2+} ions, and the N lobe on *top*, bound by two Ca^{2+} ions, *colored dark gray*. Q4B (*gold*) and Q4A (*teal*) are embraced together by CaM. *B*, *cartoon schematic* depicting the crystal structure representing the overall conformation of Ca^{2+}/CaM bound to a full KCNQ4 subunit. *C* and *D*, the *expanded views* of the CaM:Q4A:Q4B structure show the interior of CaM (*gray*) interacting with the side chains of the Q4A and Q4B peptides. The peptide residues are *colored* to match the *conserved color plot* shown in Fig. 1. These interactions are clarified in the plot in Fig. S3, and *dashed circles* in the *inset* highlight the loci of the interactions. CaM residues are *labeled* in *maroon*, Q4B is *labeled* in *black*, and Q4A is *labeled* in *teal*. *E*, the backbone C-α alignment of the Ca^{2+}/CaM:Q4A:Q4B complex with the Ca^{2+}/CaM:KCNQ1AB complex (*light gray*) from PDB entry 4UMO, in which one of the two asymmetric units of the domain-swapped pair was truncated for clarity. *F*, the *expanded view* of the overlaid structures shows the difference in position of the CaM linker as it interacts with Ile^{539} (*pink CaM*) or Arg^{519} (*gray CaM*). These structures were rendered using PyMOL.

the C-lobe EF-hands, suggesting this to be more related to [Ca^{2+}] or that Ca^{2+} ions dissociate from the C-lobe upon complex formation. Contrary to these findings, the Ca^{2+}/CaM:Q3AQ2B structure (PDB entry 5J03) found Ca^{2+} coordinated in all four EF-hands formed in a crystallization buffer containing a stoichiometric ratio of [Ca^{2+}] to [CaM] of 125:1. Thus, we must admit the likely possibility that a greater stoichiometric excess of Ca^{2+} to CaM than what we and others have used is required to fully load all "loadable" C-lobe EF-hands under crystallization conditions (45). A *color plot* of crystallographic *B*-factors of the crystal structure shows the relative level of disorder, and we observe that the EF-hands III and IV map the highest disorder (Fig. S1). This higher potential for disorder in the C-lobe may arise from this trimeric configuration, a result of the C-lobe releasing previously bound Ca^{2+} ions and rendering EF-hands III and IV less important for stabilizing the structure. The preference of Ca^{2+} for the N-lobe in this CaM-ion channel co-crystal structure is consistent with the N-lobe, not the C-lobe, being obligatory for CaM function as the Ca^{2+} sensor that regulates channel opening (57), but as our model in Fig. 10 illustrates, does not mean that the C-lobe is not the first lobe to load Ca^{2+} ions.

Similar to the other published Ca^{2+}/CaM:KCNQ structures, our crystal structure shows the A and B domains adopting helical conformations in the presence of Ca^{2+}-loaded CaM. Taking the CD spectra into account, we suggest that CaM *imposes* α-helical structure on the A and B domains of KCNQ channels. The structure shows CaM wrapped around the A and B domains, assembled into a coiled-coil configuration in antiparallel orientation, with the N-lobe bending around the B domain and the C-lobe folded around the A domain (Fig. 2, *A–E*). Comparison of the CaM backbone alignment between this structure (Protein Data Bank entry 6N5W) and the Ca^{2+}/CaM:KCNQ-AB structures published to date (PDB entries 4UMO, 4V0C, 5J03, 6FEG, 6FEH, 6B8M, 6B8N, and 6B8P) yields an RMSD range of 0.98–1.68 Å overall, with 1196–1226

atoms included in the calculation using PyMOL. An interaction plot summarizes multiple van der Waals (nonbonded contacts) in addition to several hydrogen bonds and salt bridges that hold CaM together with the A and B domains (Fig. S2). The residues involved in these interactions are indicated by *circles above* the residues in the conserved alignment panel in Fig. 1*B*. This interaction profile is almost identical, as shown, with that reported previously (48) and suggests a high degree of similarity with most of the other structures of Ca^{2+}/CaM interacting with KCNQ1–5. A notable exception is the reported structure of Ca^{2+}/CaM interacting only with the KCNQ4 B domain (48, 49). Expanded representations of the interior of the Ca^{2+}/CaM:Q4A:Q4B co-crystal structure obtained here reveal that these interactions of the A and B domains occur with the two loops within the N- and C-lobes and the N-lobe–C-lobe linker region of CaM (Fig. 2, *C* and *D*). We also observed that the more highly conserved residues of A and B domains (*pink* and *orange residues*, *colored* according to the *scale* in Fig. 1*B*) tend to face the interior of CaM rather than facing toward each other.

An overlay of this structure with the KCNQ1-AB domain-swapped complex (PDB entry 4UMO) (Fig. 2*E*) (RMSD = 1.68 Å) indicates that the only noticeable difference in these interactions localizes to the N-lobe–C-lobe linker of CaM. The expanded view reveals that Ile^{539} of Q4B allows the CaM linker to have closer contact with the B domain (Fig. 2*F*). The bulker side chain of the KCNQ1 homolog, Arg^{519}, appears to push the linker further away from the B domain. Whether this small structural difference translates to explaining the functional differences between CaM actions on KCNQ1 and KCNQ4 channels remains to be seen. Overall, these data, featuring the assembly of independent proteins, confirm that the peptides interact with Ca^{2+}/CaM similarly to the co-expressed pre-assembled AB proteins with CaM.

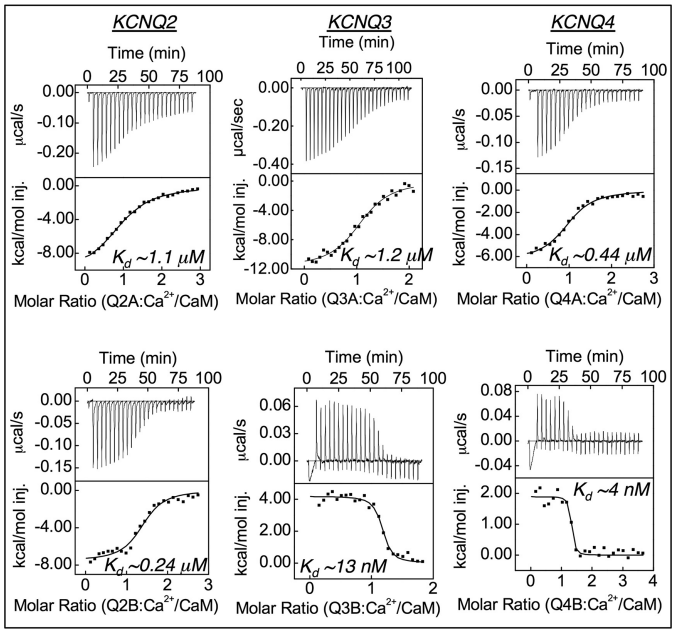

Figure 3. The B domain of KCNQ2–4 has a very high affinity for Ca^{2+}/CaM, whereas that of the A domain is modest. Isotherms are shown for the peptides (50–100 µM) titrated into 5 mM CaM in the presence of 5 µM Ca^{2+}. The A domain peptides are represented in the *top row*, and the B domain peptides are shown in the *bottom row*, representing KCNQ2, KCNQ3, and KCNQ4 isoforms. Analysis was performed using the one-site binding model in MicroCal Origin version 7.

Ca^{2+}/CaM binds the B domain with higher affinity than the A domain

We wondered whether there might be an obligate "stepwise" mechanism of complex formation between CaM and the A and B domains. The direct biochemical binding affinity of full-length CaM for each KCNQ domain individually has not been reported, although indirect measurements of apparent affinities indicate that Ca^{2+}/CaM binds the A domain of KCNQ2 in the nanomolar range (39, 58). We used isothermal titration calorimetry (ITC) to assess the thermodynamic parameters of Ca^{2+}/CaM interactions with the A and B domains of KCNQ2–4. Peptides corresponding to the A domains each displayed a moderate binding affinity for Ca^{2+}/CaM, with K_d values of ~0.44–1.2 µM (Fig. 3 (*top*) and Table 1). The B domain peptide of KCNQ2 also displayed a moderate affinity for Ca^{2+}/CaM (K_d ~0.24 µM). The B domains of KCNQ3 and KCNQ4, however, bound to Ca^{2+}/CaM very tightly, with K_d values between 4 and 13 nM (Fig. 3, *bottom*). The stoichiometry for Ca^{2+}/CaM binding to each peptide was near 1:1, with any differences explainable by remaining uncertainty in the precise peptide concentrations. Although we find here that fully Ca^{2+}-loaded CaM has far greater affinity for the B domain *versus* the A domain when present alone, when together, Ca^{2+}-loaded CaM must strongly interact with both the A and B domains. Because the crystal structures show that a single CaM embraces the A and B domains together, the very different affinities of the two domains are consistent with there being a specific order to

Table 1

Summary of ITC results of KCNQ A and B domain peptides binding Ca^{2+}/CaM

Values are mean ± S.D.

Peptide	N (# trials)	Ka (M^{-1})	Kd (µM)	N (stoichiometry)	ΔH (Kcal mol^{-1})	ΔS (cal $mol^{-1}deg^{-1}$)
Q2A	3	9.4 E+5 ± 3.1 E+02	1.08 ± 0.17	1.08 ± 0.07	-3.65 ± 4.4	-6.5 ± 4.2
Q2B	3	4.3 E+6 ± 9.9 E+02	0.24 ± 0.05	1.06 ± 0.08	-9.69 ± 1.1	-4.1 ± 4.2
Q3A	3	8.3 E+5 ± 3.9 E+05	1.22 ± 0.18	1.04 ± 0.16	-9.17 ± 4.9	-14.0 ± 1.5
Q3B	3	7.7 E+7 ± 6.2 E+03	0.013 ± 0.003	0.94 ± 0.13	3.53 ± 0.53	47.9 ± 1.9
Q4A	3	2.3 E+6 ± 5.7 E+02	0.44 ± 0.07	1.10 ± 0.11	-5.57 ± 0.25	10.3 ± 0.9
Q4B	3	4.6 E+8 ± 1.8 E+04	0.004 ± 0.003	1.04 ± 0.03	2.12 ± 0.45	44.7 ± 0.4

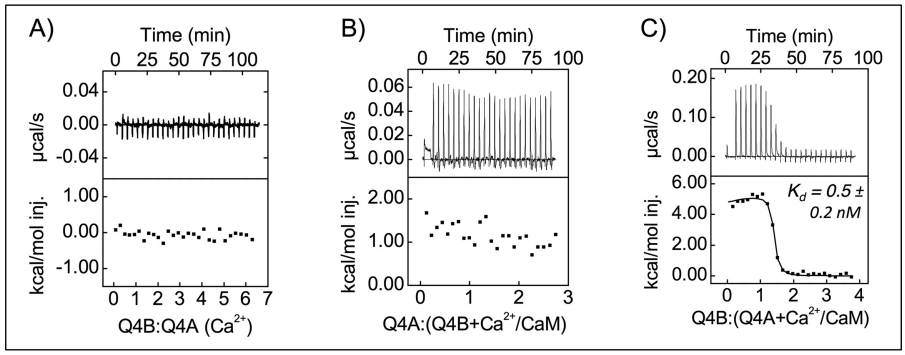

Figure 4. ITC reveals that the A domain must bind CaM first to form a stable Ca^{2+}/CaM:Q4A:Q4B trimeric complex. *A*, the shown isotherm demonstrates no detectable binding between the A and B domains in the absence of CaM. *B*, the plot of Q4A to the preformed complex of Ca^{2+}/CaM+Q4B indicates no detectable interaction. *C*, the isotherm showing the addition of Q4B to the preformed complex of Ca^{2+}/CaM+Q4A revealed a $K_d = 0.5 \pm 0.2$ nM (mean ± S.D., $n = 2$). Curve fitting was performed using the competitive model in Origin version 7.

how CaM induces formation of this trimeric complex. This is one of the central advances of this work.

Formation of the Ca^{2+}/CaM:Q4A:Q4B complex necessitates a highly ordered mechanism

Additional ITC experiments were performed to further characterize the interactions between Ca^{2+}/CaM and peptides of the KCNQ4 A and B domains (Q4A and Q4B peptides) simultaneously. First, we tested whether the A and B domains have the ability to interact in the absence of CaM. We did not observe any evidence of binding between the A and B domains using ITC (Fig. 4*A*), and we also did not observe any crystals formed of only Q4A and Q4B peptides. Both suggest that CaM is necessary to bring these two domains together. Next, we tested whether Ca^{2+}/CaM must bind the A domain or the B domain first to form a stable trimeric complex. We found that Q4A did not display a measurable interaction with a preformed complex of Ca^{2+}/CaM+Q4B (Fig. 4*B*). Reversing this order, however, showed Q4B to bind to the preformed complex of Ca^{2+}/CaM+Q4A with very high affinity ($K_d = 0.5 \pm 0.2$ nM) (Fig. 4*C*), even higher than of Q4B binding to Ca^{2+}/CaM alone. This is congruent with the data of Xu *et al.* (49), who suggested that CaM may be required to interact with the A domain first to form the trimeric complex with the B domain and who reported a putative structure of Ca^{2+}/CaM wrapped around the B domain only. Although we conclude that the ultimate configuration of Ca^{2+}-loaded CaM is wrapped around both domains, we cannot rule out the possibility that Ca^{2+}/CaM is wrapped around solely the B domain, under certain conditions that we do not yet know. Combining these data with our above ITC experiments, we suggest that an "energy barrier" must be overcome to form the trimeric complex: Ca^{2+}/CaM first binds the "lower affinity" A domain *before* binding the "higher affinity" B domain to form the trimeric complex. This would imply that for Ca^{2+}/CaM to form a fully functional complex with both the A and B domains of KCNQ4 channels, a mechanism must be in place to ensure the proper order of binding.

ApoCaM binds the B domain but not the A domain of KCNQ4

We were not able to obtain a crystal of apoCaM with the separate KCNQ4 A and B domains in our screens, as mentioned above. Additionally, our ITC data showed the Q4A to display negligible interaction with apoCaM or a preformed complex of apoCaM+Q4B in buffer containing 1 mM EGTA (Fig. S3, *A* and *B*). However, we noticed weak interactions between Q4B and apoCaM, characterized by an increase in endothermic heat exchange followed by a decrease in the endothermic profile (Fig. S3*C*). A similar isotherm was observed for Q4B binding to apoCaM+Q4A (Fig. S3*D*), indicating that apoCaM might weakly interact only with the B domain and not the A domain. Because we were unable to accurately determine a binding constant from these ITC data due to limited amounts of these proteins, we turned to microscale thermophoresis (MST), which requires a much smaller quantity of protein. We examined the interaction of fluorescently labeled apoCaM (200 nM) with Q4A or Q4B in chelexed buffer (ChHBS) supplemented with 0.5 mM EGTA, ensuring that this low concentration of CaM was wholly free of Ca^{2+}. These experiments revealed that apoCaM interacts with the B domain of KCNQ4 with a K_d of ~10 μM (confidence interval 6–17 μM; Fig. 5*A*), which is within the range of free [CaM] in cytoplasm under very low [Ca^{2+}] conditions. Similar to our ITC results, the MST experiments suggest that the A domain does not interact with apoCaM (Fig. 5*B*).

The C-lobe of the apoCaM is loosely associated with the KCNQ4 B domain

We used solution HSQC-NMR to track interactions of apoCaM with Q4A and Q4B. Spectroscopy was performed using [^{15}N]apoCaM and Q4A and Q4B in 1 mM EGTA. Peptides were added to a slight excess of 150 μM CaM based on the 1:1 stoichiometry we had observed by ITC under high-[Ca^{2+}] conditions. Fig. 6*A* shows the NMR spectrum of isolated apoCaM, with expanded regions (Fig. 6, *B–D*) comparing critical spectral peaks of apoCaM before and after the addition of Q4A and Q4B. This apoCaM spectrum closely matches the assignments of the vertebrate apoCaM spectrum shared by John Putkey (UT Health, Houston TX), further confirming that the starting CaM was indeed in the Ca^{2+}-free state. The addition of Q4A did not cause any chemical shifts or peak alterations to those of isolated apoCaM (Fig. 6*B*). In contrast, the addition of Q4B induced obvious changes to the apoCaM spectrum, revealing the apoCaM residues affected by interaction with the B domain. We observed significant changes in peaks corresponding to res-

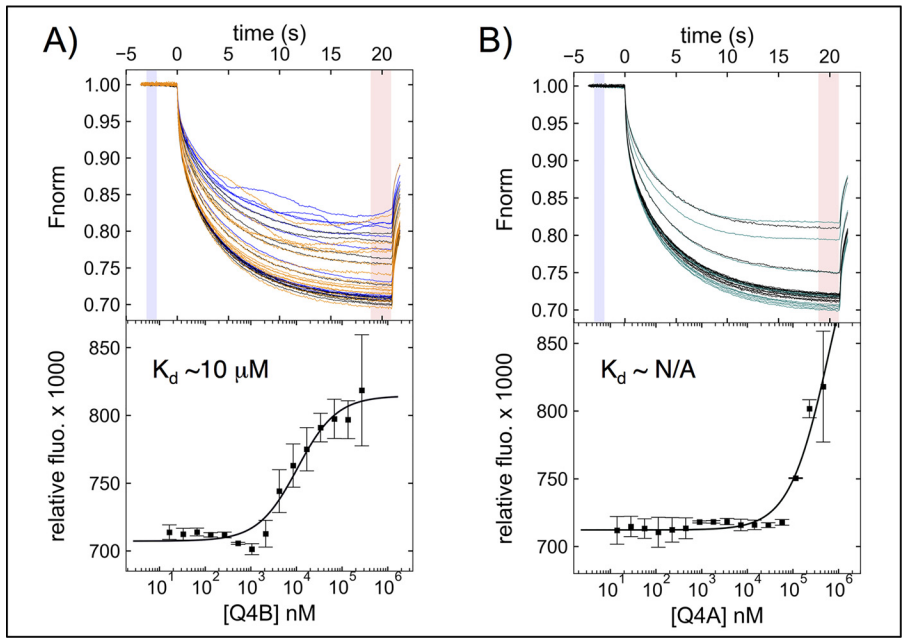

Figure 5. MST analysis of apoCaM affinity for Q4B and Q4A peptides. Titration plots are shown at the *bottom* for Alexa Fluor 594–tagged apoCaM (200 nM), titrated with Q4B (*A*), up to 220 μM, which displayed a K_d = 10 μM (confidence interval 6–17 μM, n = 3), compared with Q4A (*B*), which was too weak to determine an accurate equilibrium constant (n = 2). The normalized fluorograms are shown at the *top*, with the analyzed time points *highlighted* in *light blue* and *light red*, including Tjump + thermophoresis activity in the analysis. Five traces exhibiting high levels of aggregation were excluded. Data were analyzed using PALMIST software, and the figures were created using GUSSI software. *Error bars*, S.D.

idues Ala^{88}, Asn^{97}, Ile^{100}, and Ser^{101} and between Asp^{131} and Glu^{139}, as shown in the expanded region in Fig. 6*C* and the full spectrum in Fig. S4. The addition of Q4B to the solution containing apoCaM+Q4A (Fig. 6*D*) caused nearly identical chemical shifts or alterations to the spectral peaks of apoCaM+Q4B, further suggesting that the B domain alone is responsible for interactions with apoCaM. To determine the loci of apoCaM interactions with the B domain, we mapped the residues displaying significant chemical peak alterations observed from the above experiment onto an existing solution NMR structure of apoCaM (PDB entry 1DMO) (5). That analysis unequivocally revealed the C-lobe of apoCaM to interact with the B domain of KCNQ4 (Fig. 6*E*). Specifically, the residues that were most affected by the Q4B titrations localized to EF-hands III and IV. We plotted those significant changes in peak height, or line broadening, to Q4B titrated over a range of concentrations, which yielded $K_d = 16 \pm 5$ μM (Fig. S5). Although peak height is not a widely accepted method to determine equilibrium constants, as line broadening is not a direct report of binding, this result is very similar to that obtained using our MST experiments in Fig. 5, thus confirming by two distinct approaches that apoCaM binds the KCNQ4 B domain with a moderate affinity consistent with known cellular physiology. Based on these results, the *schematic* in Fig. 6*F* represents our interpretation of the structural interaction between apoCaM and a single KCNQ4 subunit at resting cytoplasmic [Ca^{2+}]. It suggests a conformation of the apoCaM:KCNQ4 complex quite distinct from our Ca^{2+}-loaded crystal structure (Fig. 2) and others (45, 46, 50), of Ca^{2+}/CaM in complex with the A and B domains of KCNQ1–4, and the cryo-EM structure of Ca^{2+}/CaM:KCNQXem (47), which all show the B domain interacting with the N-lobe of CaM and the A domain embraced by the C-lobe. These results challenge our initial supposition that apoCaM would be constitutively bound to the A domain and suggest a much more dynamic mechanism of Ca^{2+} directing CaM interactions with KCNQ4 channels. The implications of these results are discussed below.

Lobe switching of CaM occurs with half-loaded EF-hands

The above findings imply that a rise in [Ca^{2+}] causes a dramatic lobe switching between CaM and the KCNQ4 A and B domains. To test this hypothesis, we performed HSQC-TROSY experiments over a range of [Ca^{2+}] designed to cover <1% loading of the four EF-hands of CaM to that maximal. To avoid competition between EGTA and CaM for Ca^{2+}, we carefully controlled for [Ca^{2+}], using ChHBS in the absence of EGTA as our starting "zero-Ca^{2+}" buffer. This allows a molar stoichiometry of [Ca^{2+}]/[CaM] of no more than 1:100, resulting in an apoCaM spectrum almost identical to the spectrum of apoCaM in HBS buffer + 1 mM EGTA (Fig. S6). We monitored changes of the emission spectrum of double-labeled, deuterated CaM ([^{2}H-^{15}N]apoCaM) (50 μM), which allows better resolution of the spectrum, requiring lower protein concentration than the single-labeled [^{15}N]apoCaM used in the earlier experiments. The better resolution was necessary to track changes in the CaM and CaM+Q4B spectra over increasing Ca^{2+} titrations.

With the first addition of Ca^{2+} at 1:4 stoichiometry (1 Ca^{2+} ion/4 EF-hands), we observed obvious changes in the peaks of isolated CaM as the spectra displayed little overlap (Fig. 7 (*A–C*), *green* and *purple peaks*). At higher ratios of Ca^{2+}/EF-hands, more peaks began to overlap due to fewer peak shifts or changes, indicating less response to increased [Ca^{2+}] as the EF-hands became more loaded (Fig. 7 (*A–C*), *purple* and *orange peaks*). This suggests that CaM on its own is very responsive to small rises in [Ca^{2+}]. In contrast, CaM+Q4B displayed much

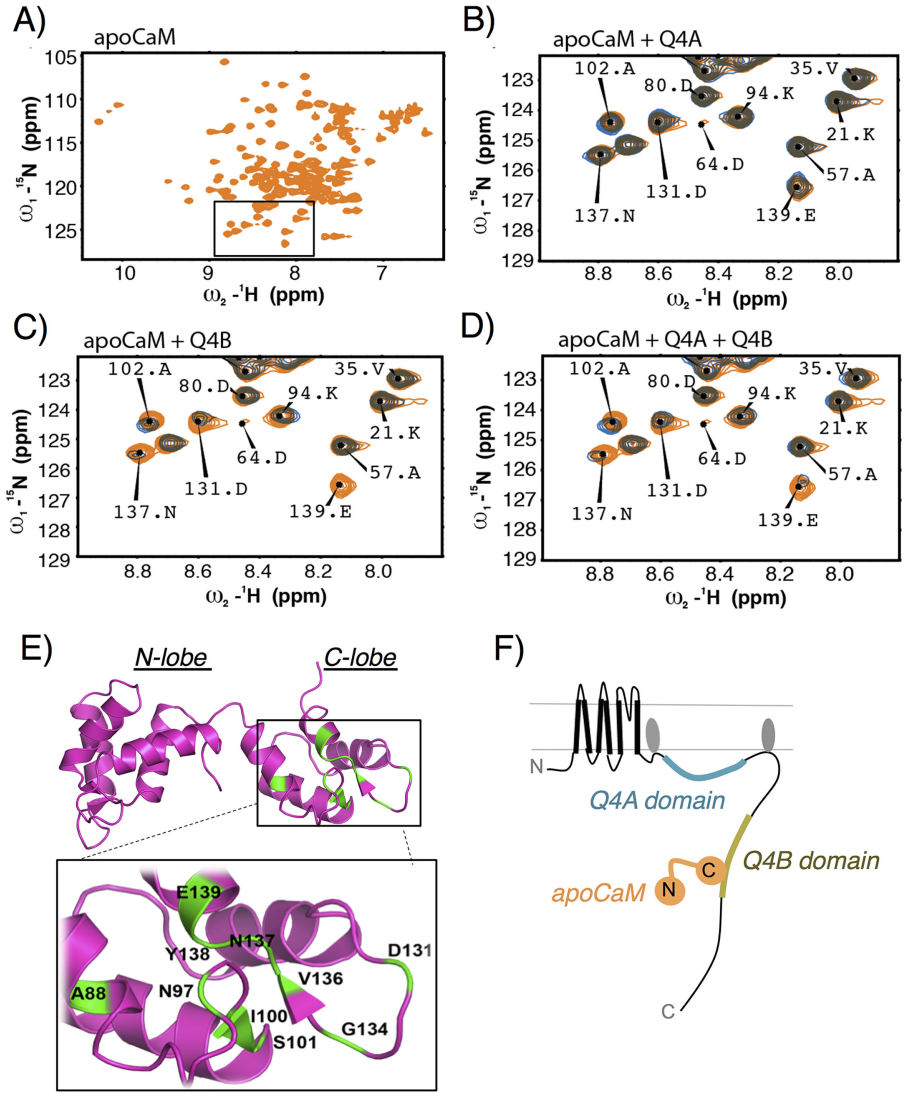

Figure 6. HSQC-NMR analysis shows changes in the apoCaM spectrum when combined with Q4B, but not Q4A. The full spectrum representing 150 μM ^{15}N-labeled apoCaM (in 1 mM EGTA) is shown in *A*. The spectra in *B–D* are expanded regions of the *boxed region* of the full spectrum, comparing apoCaM before (*orange spectrum*) and after titration with Q4A, Q4B, or both peptides (*blue spectra*) at a ratio of 1:1.2. *E*, solution NMR structure of apoCaM (PDB entry 1DMO, conformation 27) with an expanded view of the C lobe. The *green*, *labeled regions* represent residues with peak changes greater than 2 S.D. values above the mean peak height after addition of Q4B to apoCaM. *F*, *schematic* depicting a possible model of the C lobe of apoCaM (*orange*), interacting with only the B domain (*gold*) of a single KCNQ4 subunit, with A and B domains in a nonhelical state.

spectral overlap at a 1:4 ratio of Ca^{2+} to EF-hands, observed as very few changes in the peaks (Fig. 7 (*D–F*), *green* and *purple peaks*). At the point of half-loading of Ca^{2+} to the EF-hands (2:4 stoichiometry), the CaM+Q4B spectrum displayed a sudden shift, observed by the separation of *orange peaks* from the *purple peaks*. A graphical plot is shown summarizing the significant peak changes of CaM and CaM+Q4B with each addition of Ca^{2+} (Fig. 7*G*). Overall, we suggest that Q4B changes the relationship between CaM and [Ca^{2+}]. When apoCaM is bound to Q4B, more Ca^{2+} is needed to cause a change in the configuration of CaM.

We were able to track many of the amino acid residues from "zero" Ca^{2+} (0:4) up to a ratio of 2:4 or 3:4 Ca^{2+}/CaM EF-hands. Although more shifts were observed in the spectra, as previously noted in Fig. 7, only those residues that changed in position >55% from the previous titration, and that we could track from the initial zero [Ca^{2+}] spectrum, are plotted. Fig. 8*A* shows that those residues localize to both lobes of apoCaM changed over the range of 0:4 to 1:4 Ca^{2+}/CaM EF-hands, and even more residues localized throughout the protein changed at a 2:4 stoichiometry (Fig. 8*B*).

Interestingly, in the presence of Q4B, only the C-lobe residues of CaM+Q4B displayed peak alterations over a range from 0:4 to 1:4 Ca^{2+}/CaM EF-hands (Fig. 8*C*). This suggests that Ca^{2+} binds CaM first to the C-lobe of Q4B-bound CaM. As shown in Fig. 6, the C-lobe interacts with Q4B in the absence of Ca^{2+}, so this finding also suggests that Ca^{2+} may displace Q4B from the C-lobe. At a 2:4 stoichiometry, residue emissions shifted throughout the CaM protein (Fig. 8*D*), followed by changes mostly within the N-lobe upon further increases of Ca^{2+} molar ratio (Fig. 8*E*). Fig. 8 illustrates our interpretation of the changes of CaM structure in relation to the B domain, based on these NMR data. The coordinated response of CaM to Ca^{2+}, in which responding residues shift from the C-lobe

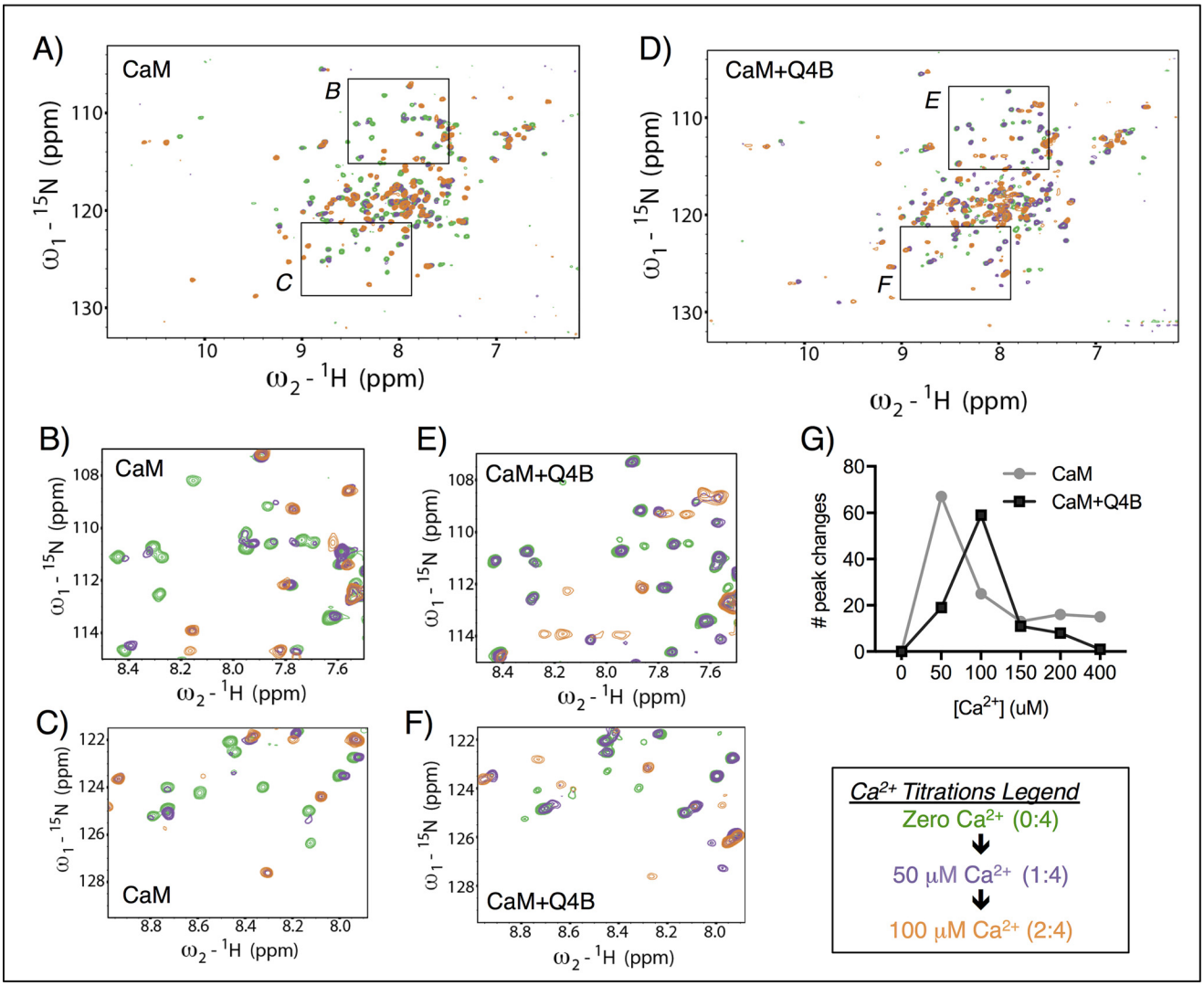

Figure 7. TROSY-HSQC-NMR analysis of the relationship between molar ratio of Ca^{2+}/CaM or Ca^{2+}/CaM+Q4B and alterations in apoCaM residues. Shown is the full NMR spectrum of 50 μM [^{1}H-^{15}N]CaM (*A*) or 50 μM [^{1}H-^{15}N]CaM + 62.5 μM Q4B (*D*), in which the *green peaks* are from residues of the metal-free protein in ChHBS, *purple peaks* are those upon the addition of 50 μM Ca^{2+}, and *orange peaks* are from residues upon the addition of 100 μM Ca^{2+}. The *labeled boxes* in the full spectrum images refer to the expanded regions in which *B* and *C* correspond to Ca^{2+} titrated to CaM only, and *E* and *F* are expanded regions of the Ca^{2+} titrations to CaM+Q4B. Those peaks showing overlapping residues are those that were unaffected by the added Ca^{2+}, indicated in *color*. In contrast, peaks that do not overlap in *color* indicate a change in the spectral peak of the corresponding residue with the addition of Ca^{2+}. *G*, *graphical representation* of the total number of peak height changes of the single NMR titration >55% above the mean peak height after each titration of Ca^{2+}. Because we could no longer track peaks from the previous titrations at 200 μM, we included all peak changes counted by visual inspection for 200 and 400 μM Ca^{2+}. The *box* at the *bottom right* shows the expected molar ratios of Ca^{2+}/CaM EF-hands in each case.

to the N-lobe when Q4B is prebound to apoCaM, again contrasts with the behavior of isolated CaM in response to [Ca^{2+}]. These findings suggest that Ca^{2+} induces CaM to dissociate completely (although probably extremely briefly) from the KCNQ4 B domain to allow the C-lobe to bind to the KCNQ4 A domain. If true, then this dissociation explains the intermediate step involving the C-lobe of CaM translocating from the B domain under "zero" [Ca^{2+}] to the A domain of KCNQ4 under higher [Ca^{2+}]. We conclude that 1) Ca^{2+} ions interfere with Q4B interactions with apoCaM; 2) Ca^{2+} ions initially load the C-lobe of the apoCaM:Q4B complex, instead of the N-lobe; and 3) a highly coordinated sequence of binding-unbinding-rebinding steps occurs over a physiological range of very low to high [Ca^{2+}], which we here refer to as a "lobe-switching mechanism." We elaborate on this in Fig. 10.

Ca^{2+}/CaM-mediated inhibition of KCNQ4 channels is not associated with shifts in voltage dependence

Regarding the CaM-mediated inhibition of KCNQ channel gating by rises in [Ca^{2+}]$_i$, there have been conflicting reports of this action involving shifts of the voltage dependence of activation or changes in gating kinetics. Studying endogenous M current in sympathetic neurons or cloned KCNQ2/3 heteromers or KCNQ2–5 homomers, our group has not ever observed any changes in activation or deactivation kinetics induced by any form of CaM over the full range of physiological [Ca^{2+}]$_i$ (7, 57). There are two alternatively spliced isoforms of human KCNQ4, called KCNQ4a and KCNQ4b, displaying very distinct activation kinetics. Most laboratories, including ours, have used KCNQ4a, which we and others call "KCNQ4." Xu *et al.* (59) found overexpression with KCNQ4a of a "dominant-negative"

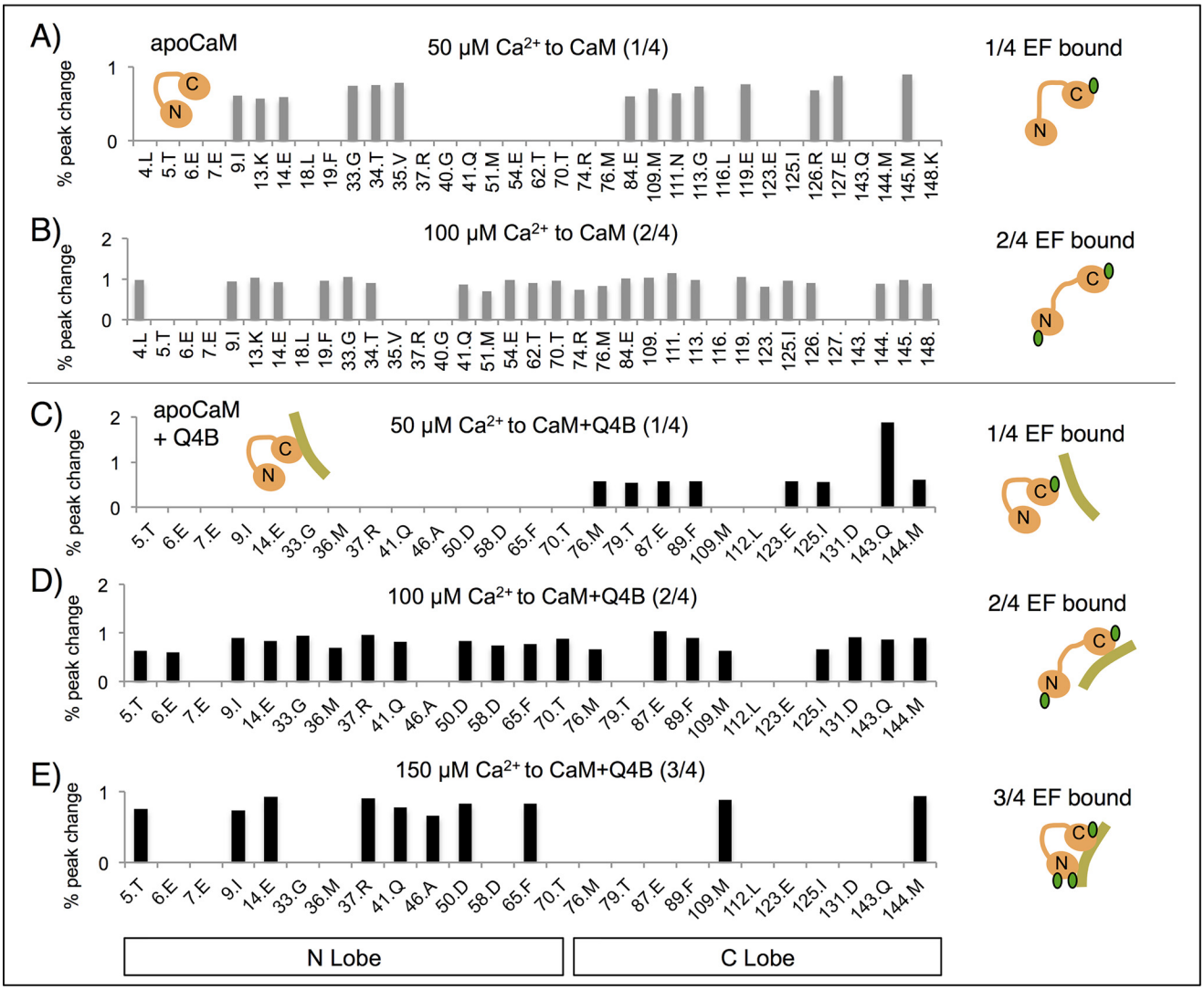

Figure 8. Graphical plot of CaM residues displaying changes in spectral peaks over the range [Ca^{2+}] titration series of molar ratios of Ca^{2+}. HSQC-NMR peak heights that changed >55% from the previous titration of Ca^{2+} to 50 μM [^{2}H-^{15}N]CaM or 50 μM [^{2}H-^{15}N]CaM + 62.5 μM Q4B starting in ChHBS, are represented by the *gray* or *black bars*. Only peaks that could be tracked from the original apoCaM position are shown. *A* and *B*, significant peak changes of peptide-free CaM in response to Ca^{2+} at a ratio of 1:4 EF-hands (*i.e.* 50 μM Ca^{2+} to 50 μM total CaM in *A* or 2:4 EF-hands in *B*). The same analysis was performed for Ca^{2+} titration into CaM + Q4B ranging up to 150 μM Ca^2 (*C*, *D*, and *E*). *Cartoon schematics* are shown with each plot, to show the estimated stoichiometry of Ca^{2+} ions (*green ovals*) with respect to the EF-hands and our speculated movement of CaM (*orange dumbbell*) with respect to the Q4B peptide (*thick gold line*). The *schematics* on the *right side* of the graph represent metal-free CaM and CaM + Q4B before the addition of Ca^{2+}.

CaM, in which all four EF-hands have been mutated to be incapable of loading Ca^{2+} ions, shifted the voltage dependence of activation by ~−36 mV. Other laboratories have reported much more modest changes of voltage dependence of ~10 mV for KCNQ2 or KCNQ3 homomers or KCNQ2/3 heteromers, with only minor changes in kinetics (30, 60–62). The case of KCNQ1-containing channels is unique in that 1) Ca^{2+}-loaded CaM augments currents from those channels, instead of depressing them (34), and 2) the S2-S3 linker of KCNQ1 is wholly nonconserved with that of KCNQ2–5. Indeed, a cysteine triplet conserved among the latter is the site of reactive oxygen species, whose action dramatically increases the opening of KCNQ2, KCNQ4, and KCNQ2/3, but not KCNQ1-containing channels (63–65), whereas the S2-S3 linker of KCNQ1 has been recently suggested to gently engage bound CaM, resulting in shifts in voltage dependence of those channels also by ~10 mV (47). A recent crystal structure of apoCaM with the joined A and B domains of KCNQ4 suggested a very large lobe-specific action of CaM on the voltage dependence of activation of KCNQ4, by >35 mV, and a strong effect on activation kinetics ~3.4-fold in magnitude (48). Because that group coupled such dramatic effects on voltage dependence and kinetics with their suggested structural model and were so divergent from our previous studies (7, 57), we decided to revisit this issue.

Chinese hamster ovary (CHO) cells were co-transfected with KCNQ4 and either WT CaM, CaM(1,2), CaM(3,4), or CaM(1,2,3,4), where CaM(1,2) and CaM(3,4) refer to N- or C-lobe mutants that cannot bind Ca^{2+} ions in that lobe, respectively, and CaM(1,2,3,4) (*i.e.* D20A/D56A/D93A/D129A) cannot bind Ca^{2+} in either lobe. All of the constructs, which were the same cDNA as used previously by us (57), were resequenced in their entirety and found to be correct. As before, we performed experiments in the perforated patch variant of whole-cell voltage clamp and, moreover, ensured that the resulting

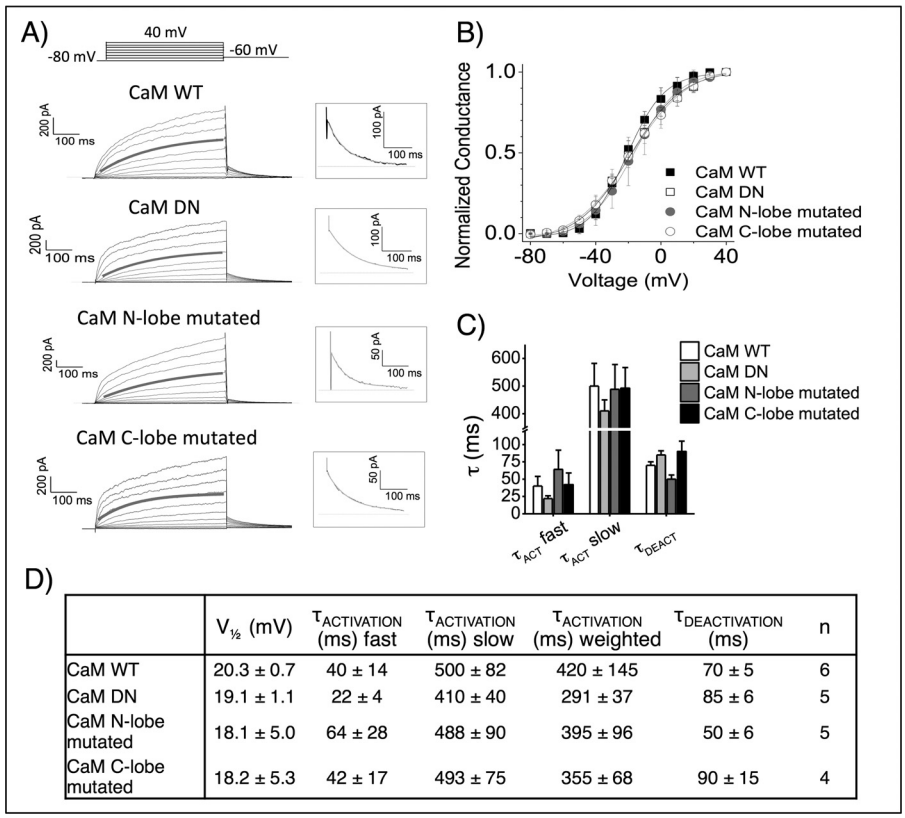

	$V_{½}$ (mV)	$\tau_{ACTIVATION}$ (ms) fast	$\tau_{ACTIVATION}$ (ms) slow	$\tau_{ACTIVATION}$ (ms) weighted	$\tau_{DEACTIVATION}$ (ms)	n
CaM WT	20.3 ± 0.7	40 ± 14	500 ± 82	420 ± 145	70 ± 5	6
CaM DN	19.1 ± 1.1	22 ± 4	410 ± 40	291 ± 37	85 ± 6	5
CaM N-lobe mutated	18.1 ± 5.0	64 ± 28	488 ± 90	395 ± 96	50 ± 6	5
CaM C-lobe mutated	18.2 ± 5.3	42 ± 17	493 ± 75	355 ± 68	90 ± 15	4

Figure 9. WT or mutant CaM-lobe mutants do not affect the voltage dependence of KCNQ4 currents. *A*, representative perforated patch voltage-clamp recordings from CHO cells expressing KCNQ4 channels together with either WT or the indicated CaM mutants. The kinetics of activation at 10 mV and deactivation (*inset*) at −60 mV after the prepulse were quantified by fits to a double and single exponential, respectively. Fits are shown in *gray*. *B*, superimposed are the voltage-dependent activation curves for the KCNQ4 + CaM combinations shown in *A*, assayed as the amplitude of the tail current at −60 mV after the 500-ms prepulse to the indicated voltages. *C*, comparison of the activation and deactivation time constant values. *D*, a *table* summarizes the data shown in *A–C*. Overexpression of CaM WT or the indicated CaM mutants did not induce significant changes in the voltage dependence of activation or in the kinetics of activation or deactivation. *Error bars*, S.E., as these are group data.

currents were not so large as to either induce series resistance errors or "soak up" all of the PIP_2 molecules in the plasma membrane, both of which might cause artifacts in our data. Cell lysates from each group were also immunoblotted with anti-KCNQ4 or anti-CaM antibodies to ensure a reasonable balance of expression of the two proteins. We found that such cells expressed very similar currents from each group, with very similar properties (Fig. 9). For cells co-transfected with KCNQ4 and WT CaM, CaM(1,2), CaM(3,4), or CaM(1,2,3,4), the midpoint voltage of activation ($V_{½}$) values were −20.3 ± 0.7, −18.1 ± 5.0, −18.2 ± 5.3, and −19.1 ± 1.1 mV, respectively (n = 6, 5, 4, and 5). The activation kinetics at 10 mV were likewise not significantly divergent for cells in each group, having the weighted time constants (see "Experimental procedures") of 420 ± 145, 395 ± 96, 355 ± 68, and 291 ± 37 ms, respectively. Likewise, there were no significant differences in the deactivation kinetics at −60 mV, which were 70 ± 5, 50 ± 6, 90 ± 15, and 85 ± 6 ms, respectively. Whereas the modest number of cells studied does not rule out minor changes in activation kinetics in the presence of different forms of CaM, any such differences could only be small.

Discussion

The results from this study highlight several key elements of the dynamics of CaM interaction with the A and B domains of KCNQ2–4. First, we showed that the A and B domains of the channels are likely to be intrinsically disordered in the absence of CaM and that interactions with CaM Ca^{2+}-loaded in at least its N-lobe imposes α-helical secondary structure on those domains. Next, we demonstrated that apoCaM does indeed bind KCNQ4 subunits with moderate affinity with only the C-lobe of apoCaM interacting with the B domain of KCNQ4. Finally, the major advance of this work is our finding that a dramatic lobe switching of CaM interaction with the KCNQ4 A and B domain occurs from low to high [Ca^{2+}].

Despite our findings that the A and B domains are likely to be disordered in the absence of CaM, the above experiments do not allow us to conclude whether apoCaM induces the helical structure on the B domain, a question planned for future studies. However, the co-crystal structures of KCNQ A-B with CaM all clearly show the A and B domains helical, whether in the presence of divalent cations, such as Mg^{2+} or Ca^{2+}, or after removal of either divalent from the preformed structure (48). This induced conformational change in CaM target proteins has been widely observed, such as for Ca^{2+}/CaM-dependent kinases (66) and other ion channels (53, 66–68). Our finding that apoCaM binds the B domain might account for the obligatory need for the presence of CaM reported by several laboratories either for functional expression of KCNQ channels or

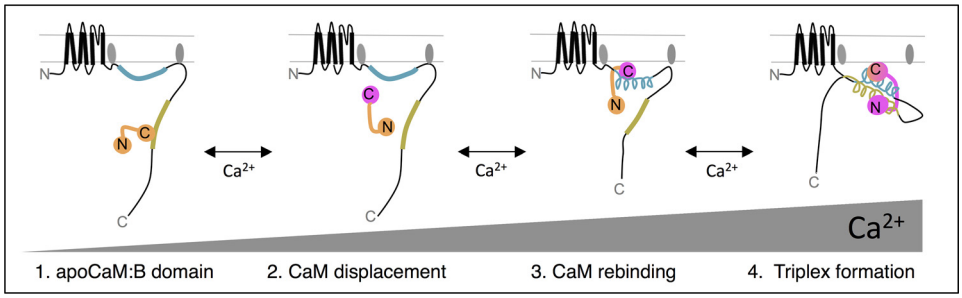

Figure 10. Proposed "lobe-switching model" for CaM regulation of neuronal KCNQ channels. Shown *schematically* is our proposed model of how Ca^{2+} ions direct CaM in interactions with, and regulation of, neuronal KCNQ channels. We here exclude the likely role of Mg^{2+} or other ions, as discussed under "Discussion." *1*, under very low (<10 nM) cytosolic [Ca^{2+}] (a physiological state that we cannot determine), apoCaM is prebound to the B domain (*gold section* of KCNQ subunit), and the NMR and MST data derive a K_d of ~10–20 μM. During this state, the PIP_2 interaction sites within the proximal C terminus at the S6Jx (pre-A helix) and the A-B domain linker are available to interact with PIP_2. Under such conditions, the A and B domains are likely disordered, not in a helical conformation, and it is still unclear whether this conformational state would represent a functional channel at the plasma membrane, where PIP_2 is located. *2*, when $[Ca^{2+}]_i$ is in the range of that in cytoplasm in neurons at rest, Ca^{2+} first binds the EF-hands of the C-lobe (indicated by the change in *color* from *orange* to *pink*), displacing CaM from the B domain. *3*, upon a rise in [Ca^{2+}] in the proximity of the channel, the Ca^{2+}-bound C-lobe binds to the A domain with a K_d of ~400 nM, inducing an α-helical conformation to the A domain (*cyan*, now shown as a *helix*). This twisting motion may impose torque on the PIP_2 interaction sites in the proximal C terminus, partially weakening their interactions with PIP_2. *4*, in the final step, under a strong [Ca^{2+}] signal (such as strong stimulation of certain $G_{q/11}$-coupled receptors), the EF-hands of the N-lobe become occupied by Ca^{2+} ions, enhancing its affinity for the B domain, inducing it into a helical formation, retaining C-lobe binding to the A domain (still a helix). This final twisting motion may completely twist or pull away the PIP_2 interaction sites from the inner leaflet of the membrane, severely hindering the ability of the C terminus to bind PIP_2, resulting in maximal Ca^{2+}/CaM-mediated inhibition of neuronal M channels. The subnanomolar affinity of the CaM:A+B trimeric complex may allow Ca^{2+} ions to rapidly move in and out of EF-III and -IV while maintaining a stable complex during such elevated [Ca^{2+}] conditions; thus, accounting for crystals variably observed to contain Ca^{2+} ions in the C-lobe EF-hands.

their assembly in the plasma membrane of either tissue culture cells or neurons (28, 34, 37, 39, 60). The reason likely has to do with the obligatory interactions of all KCNQ channels for interactions with PIP_2 in the plasma membrane for function (69, 70). Given that the two most important domains of the channels for PIP_2 interactions are in the proximal C terminus (Fig. 10) (41, 46, 71), such a change in structure may prevent the RD from stable interactions with PIP_2 (30), thus hindering opening. Another group has also shown an intricate relationship between channel interactions with PIP_2 and CaM (44). However, as opposed to test tube experiments, all cells, especially excitable cells, express CaM at high levels in cytoplasm. As CaM is increasingly Ca^{2+}-loaded in response to increasing $[Ca^{2+}]_i$, we propose that the tight embrace of the A and B domains (now certainly helices) condenses the RD to a springlike structure, pulling it away from the plasma membrane and interfering with those KCNQ-PIP_2 interactions, thus causing suppression of M current. We present our model in more detail in Fig. 10.

To properly interpret our data, we must consider the physiology of CaM molecules and Ca^{2+} ions in the cytoplasm. Because the affinity of CaM for almost all of its cellular targets greatly increases upon Ca^{2+} loading (neurogranin being a notable converse example (6, 72–74)), free [CaM], either Ca^{2+}-bound or not, is exquisitely dependent upon $[Ca^{2+}]_i$, with *available* CaM ranging as high as perhaps 40 μM at the lowest conceivable values of free [Ca^{2+}] in the cytoplasm, down to <10 nM upon high elevations in global [Ca^{2+}] (75–77), such as in response to strong neuronal stimulation and rapid firing. It is important to note that, unlike the case of CaM actions on VGCCs, for which highly local free [Ca^{2+}] at the inner mouth of the pore may approach millimolar concentrations (16, 78, 79), no Ca^{2+} ions are flowing through open K^+ channels, and so it is likely that, as for the analysis of CaM actions on SK K^+ channels, it is global [Ca^{2+}] that should be most relevant for our thinking. This supposition is tempered, however, by the discovery of KCNQ channels and Ca^{2+}-permeable channels clustered together in microdomains in sensory neurons (80), and similar multichannel complexes likely exist in brain as well (81–83). Thus, we cannot say with certainty the precise [Ca^{2+}] in the local micro-environment of KCNQ channels in nerve, heart, and muscle that corresponds to CaM being maximally "switched on."

Studied in isolation via ITC, we found Ca^{2+}/CaM to have a much higher affinity for the B domains than for the A domains of KCNQ2–4, with KCNQ3 and KCNQ4 most notably so. However, the affinity increased by an order of magnitude when the A domain was present as well. Consistent with those measurements is the high-resolution crystal structure we obtained of Ca^{2+}-loaded CaM wrapped around the A and B domains, very similar to that reported earlier for a variety of KCNQ subtypes (45–47, 50). None of that work suggests a role of CaM in cross-linking the C termini of the subunits in the tetramer, but rather suggests that CaM interacts within individual subunits. A caveat to our conclusions is our ITC results, in which the addition of the A domain to a preformed Ca^{2+}/CaM-B helix complex did not induce a thermodynamic signal; thus, we cannot rule out a configuration of Ca^{2+}/CaM wrapped around the B domain alone under certain cytoplasmic conditions, as suggested by another group (48, 49). It is important to remember that absolute affinities assayed in test tube experiments with isolated A and B domains and CaM molecules are likely much different from those when the RD is attached to the rest of the channel, namely coupled to the gating machinery, as well as the changes in affinities of the EF-hands of CaM for Ca^{2+} when pre-associated with the relevant domains of the channels (18, 22, 54). However, we assert that the *relative* affinities and thermodynamic parameters are likely to parallel our findings in intact cell experiments, giving us insight into conformational changes over ranges of physiological [Ca^{2+}] and [CaM].

Our observations of the Ca^{2+} titrations shifting from emission changes in C-lobe residues to those including the N-lobe of CaM prebound to Q4B lead us to propose a lobe-switching

model. The issue of lobe dependence and/or specificity for CaM actions (both CDI and CDF) on VGCCs is represented by a vast literature that reveals surprisingly stark differences between L-type (Ca_V1) and N and P/Q-type (Ca_V2) Ca^{2+} channels. For the former, the C-lobe is recognized as the "Ca^{2+} sensor" provoking CDI, whereas for the latter, the N-lobe has been proposed to fulfill that role (16). Moreover, for both Ca_V1 and Ca_V2 channels, lobe switching has been proposed as a key structural mechanism, involving an N-terminal region of the channels (84, 85), and it is tempting to think that this CaM-mediated regulatory mechanism is conserved among channel types (86). Notably, there have not been any structural analyses of CaM/KCNQ channel interactions that include the N terminus of KCNQ channels, which have been suggested to play key roles in gating by interacting with the C terminus, involving syntaxin and CaM (62, 87). Our thinking also takes into account our earlier work indicating Ca^{2+} loading of the N-lobe of CaM to be critical for Ca^{2+}/CaM-mediated suppression of KCNQ2, KCNQ4, and KCNQ2/3 channels, with Ca^{2+} loading of the C-lobe unimportant. That work was performed on living cells expressing full-length, functional channels, studied under perforated patch whole-cell recording (57) rather than only analyses of C-terminal fragments.

We were unable to obtain a crystal of this or any other "apo" state under metal-free conditions using our crystallization screen of 1,728 conditions by assembling the discrete proteins in the absence of Ca^{2+}. Our apoCaM data contrast with a recent report showing co-expressed (pre-assembled) apoCaM co-crystallized with the AB fragment of KCNQ4 (PDB entry 6B8L) in which Ca^{2+} had been removed from the preformed complex (48) and another showing the solution NMR structure of apoCaM:KCNQ2-AB (PDB code 6FEG) that had been similarly co-expressed and purified (50). Aside from their absence of Ca^{2+} ions, these "apo" structures are still quite similar to that found for the Ca^{2+}/CaM:KCNQ-AB complexes (45–47). We note that the primary difference between these apo structures and the apo model we propose is in how the complex was assembled; in this study, we combined each Ca^{2+}-free protein/peptide separately with the crystallization buffer, whereas all others had been co-expressed and preassembled in a divalent cation-rich medium (LB/2YT) prior to removal of the Ca^{2+} ions with EGTA. We think this suggests that the complex itself is more stable than the transient Ca^{2+} state of the CaM-EF-hands.

Millet and colleagues (50) called their structure "intermediate," with regard to metal, consistent with this complex not being wholly Ca^{2+}-free, and reported that complete unloading of all Ca^{2+} from the preformed complexes was difficult. Under those circumstances, any further loading of Ca^{2+} ions to the complex displayed a K_d value using FRET assays of ~1 μM (50), a value similar to that globally in the cytoplasm of neurons in response to a stimulus. Our solution NMR and MST experiments suggest that the C-lobe of apoCaM weakly interacts with the KCNQ4 B domain under Ca^{2+} conditions at which at most 1% of the CaM EF-hands could be Ca^{2+}-loaded, and at extremely low $[Ca^{2+}]_i$, free CaM may be within that range in the cytoplasm (76, 77). It is unclear what physiological condition would correspond to such a scarcity of Ca^{2+} ions relative to CaM molecules, but under those conditions, we found the C-lobe of CaM to interact solely with the B domain of KCNQ4. Titration of Ca^{2+} into the apoCaM+Q4B complex measured by NMR suggests that Ca^{2+} must reach a stoichiometry of 1:4 (EF-hands) to displace the B domain from the C-lobe. Taken together, our results can only be reconciled by a profound change in the configuration of the KCNQ4 RD when CaM is half-loaded by Ca^{2+} (two of the four EF-hands bound by Ca^{2+}), under which the Ca^{2+}-loaded N-lobe now strongly interacts with the B domain with very high affinity. This configuration seems to be particularly stable, as consistently found by all investigators.

Like many studies, we here ignore the significant concentration of free Mg^{2+} ions, estimated to be ~0.5–1 mM in neurons, and given that the known affinities of Mg^{2+} ions for the CaM EF-hands are within that range, predict significant occupancy of CaM EF-hands at tonic $[Ca^{2+}]_i$ (88–90). Thus, it is likely that in resting cells at which free $[Ca^{2+}]$ is low, some or all of the EF-hands of CaM are not empty but rather are occupied by Mg^{2+} ions. The high-resolution crystal structure of the Mg^{2+}-loaded N-lobe of CaM reveals Mg^{2+} ions in both EF-hands, but in contrast with Ca^{2+} occupancy, 2–4 H_2O molecules are also included in each EF-hand (89), which could electrostatically shield much of the charge of divalent ions and perhaps alter interactions of the RD with the membrane. The occupancy by CaM by Mg^{2+} ions when CaM is "off" was explicitly assumed for the solved CaM/$Na_V1.2$/FGFHF complex (91) and recently examined for CaM/KCNQ4 RD interactions (48). This raises the likelihood of "alkali earth-metal exchange" being part of the switching of CaM "on" or "off" in its functional interactions with the channels. This topic has also been explored for the case of synaptotagmin, whose structure when loaded with Mg^{2+} (under which exocytosis is inhibited) has also been determined (92, 93). In all of these cases, the structure of the CaM/target complex was suggested to be only subtly distinct between Mg^{2+}-loaded and Ca^{2+}-loaded forms. How these results can be in accord with the indisputable role of Ca^{2+} as the "switch" for CaM actions on these proteins remains to be elucidated.

Based on our results, we propose a "lobe-switching model" in which Ca^{2+} ions compete with the B domain for binding the C-lobe under low $[Ca^{2+}]$, causing the B domain to dissociate from CaM in a stepwise CaM action on KCNQ4 channels (Fig. 10). The true "apo" configuration (Fig. 10, *1*) can only occur during extremely low (<10 nM) $[Ca^{2+}]$, and we do not know whether and when such a low value occurs in the cytoplasm of living cells, which contain up to 1 mM free $[Mg^{2+}]$. Nonetheless, in this state, the C-lobe of apoCaM binds the B domain with modest affinity, and the N-lobe of CaM and the A domain of the channel are not involved. Because the RD is in a flexible, "open" configuration, we suppose it could be anchored to the plasma membrane via the two PIP_2-binding sites located on both ends of the A domain (the "S6Jx" or "pre-A helix" site and the linker between the A and B domain). In this state, both the A and B domains are likely still disordered and nonhelical. It is unclear whether the channel can function in this fully "apoCaM" state. At local free $[Ca^{2+}]$ near resting levels in excitable cells (50–100 nM), the complex rapidly adopts a CaM displacement configuration, in which the B domain dissociates from the C-lobe and

CaM is reconfigured to a "target-ready" state that can recognize the A domain (Fig. 10, *2*). This brief state then likely quickly transitions to the CaM rebinding configuration (Fig. 10, *3*), as a result of Ca^{2+}-loaded C-lobe (half-loaded CaM) binding to the A domain, imposing an α-helical structure on the A domain and condensing the proximal C terminus. In the first three of these configurations, the RD is relatively relaxed, allowing the C terminus to extend the two proposed PIP_2-binding sites, the "S6Jx" or "pre-A helix," and the "A-B linker," to interact with PIP_2 at the plasma membrane–cytoplasm interface.

We take note, however, that our earlier work found exogenous expression of mutant C-lobe CaM that cannot bind Ca^{2+} ions to not perturb Ca^{2+}-mediated suppression of KCNQ2, KCNQ4, and KCNQ2/3, channels expressed in CHO cells (57). How can that be reconciled with our data and model here, which require Ca^{2+} ions in the C-lobe in steps 1 and 3 in Fig. 10? We think the answer lies in the extremely high affinity of Ca^{2+} ions for the C-lobe, and the presence of endogenous CaM in nearly all mammalian cells, with even more so in neurons. Thus, KCNQ channels already assembled in the Golgi (with the C termini in the cytoplasm) are prebound by endogenous CaM with Ca^{2+} ions in the C-lobe and do not lose those ions. Overexpression of C-lobe mutant CaM is very much higher than expression of endogenous CaM. However, no inhibition of neuronal KCNQ channels can occur without the Ca^{2+}/N lobe-dependent embrace of the A and B helices, which is what pulls the RD away from the plasma membrane, disrupting the obligatory interactions between PIP_2 and the two PIP_2 interaction sites in the proximal C terminus of the channels that are required for channel opening.

We hypothesize that upon a physiological signal that causes a substantial rise in free $[Ca^{2+}]_i$ in the vicinity of the "primed" CaM/RD complex, the triplex configuration occurs (Fig. 10, *4*), as Ca^{2+} binds the N-lobe of CaM, causing it to latch around the B domain. This induces a pulling/torsional Ca^{2+}-induced motion, as suggested recently (50), likely disrupting the critical interactions between the RD and PIP_2, causing inhibition of channel gating for neuronal M channels. We note that this "condensed" trimolecular configuration, as opposed to the "open" structure of free Ca^{2+}-loaded CaM, is due to its intimate interaction with the A and B helices, with which its many bonds and sites of interaction provide the energetics for the resultant tight configuration of CaM. Thus, we suggest here that both the A and B helices and CaM rearrange their secondary and tertiary structures in response to each other, similar to the "mutually induced fit" already noted for CaM interactions with Ca^{2+}/CaM kinases (66). This insight we believe to represent another advance of this paper.

Finally, with a rise in $[Ca^{2+}]$ that is more than transient, this configuration is "locked," and the double anti-parallel helical conformation of the complex is stabilized, creating a compact geometry that severely disrupts PIP_2 interactions with KCNQ C termini that likely takes some minutes to reverse, as seen physiologically. Although Ca^{2+} must be bound to the C-lobe first to displace CaM from the B domain, it is Ca^{2+} loading of the N-lobe that creates this highly stable trimeric complex, which allows freedom within EF-hands III and IV of the C-lobe, rendering their ligation of Ca^{2+} optional at this final step. Our lobe-switching model could provide the explanation for the discrepancies reported in the literature of how Ca^{2+} directs CaM in its binding to, and regulation of, KCNQ channels, as it does incorporate some role of metal loading of the C-lobe as (an early) part of the mechanism (48) but retains Ca^{2+} binding to the N-lobe as the modulatory switch, in accord with our physiological experiments in cells (57). It also is in accord with the need for CaM for functional expression (28, 39, 58). However, we do not believe that CaM interacts with the voltage-sensor domain of KCNQ2–5 channels and that as for PIP_2 actions on those channels (94), effects on voltage dependence are minimal. Future studies to test the affinities of the peptides with inactive N- or C-lobe CaM mutants and these domains will further probe whether this lobe-switching mechanism is indeed correct.

Experimental procedures

Buffers and protein preparation

Peptides corresponding to the A and B domains of KCNQ2–4 were synthesized to 95% purity (Peptide 2.0, Chantilly, VA). The lyophilized peptides were reconstituted in HBS buffer, which consists of 20 mM HEPES and 150 mM NaCl at pH 7.4, made with deionized water. We name each peptide according to the subunit isoform and the CaM binding domain: Q2A, Q2B, Q3A, Q3B, Q4A and Q4B, referring to the A or B domains of KCNQ2–4, respectively. A plasmid containing WT, untagged vertebrate CaM (plasmid pETGQ.HCaM) was a gift from William N. Zagotta (University of Washington). Vertebrate CaM was expressed in BL21 competent cells at 37 °C for 6 h in LB or minimal essential medium containing [^{15}N]ammonium chloride, depending on the experimental design, and then purified using phenyl-Sepharose matrix (GE Healthcare). For experiments requiring higher resolution of NMR spectra we expressed in D_2O (Millipore-Sigma). The eluent was further purified through a Superdex 75 column on an AKTA FPLC system (GE Healthcare). For divalent metal-free CaM (apoCaM) studies, the protein was exchanged to HBS buffer that had been soaked with Chelex reagent (Bio-Rad). We refer to this chelexed buffer as "ChHBS." Glassware and other containers used for apoCaM measurements were prerinsed with 10 mM EGTA, followed by 2× ChHBS rinses, prior to the addition of proteins. The *total* $[Ca^{2+}]$ in the ChHBS buffer was determined by inductively coupled plasma MS to be ~500 nM (Northwestern University, Evanston, IL). The peptides used for apoCaM interactions were reconstituted in ChHBS. The concentrations of the peptides and CaM were determined by amino acid analysis at the Texas A&M University Protein Chemistry Laboratory core (College Station, TX).

CD

Proteins were diluted to ~30 μM in potassium phosphate buffer (KH_2PO_4), pH 7.4, containing 5 mM NaCl and ~5–30 μM Ca^{2+} (determined by inductively coupled plasma MS and fluorescence spectroscopy using Ca^{2+} indicator dyes) and placed in a 0.5-cm path length quartz cuvette. The molar ellipticity of each peptide was reported using a Jasco J-810 CD spectrometer at 4 °C. CD spectra were recorded from 270 to 190 nm in 0.1-nm steps. The CD signals were corrected by subtracting the spectra from buffer only. The CD analysis plotting tool, CAPITO, was used to determine the predicted content of α-heli-

ces, β-sheets, and random coils of the indicated peptides and proteins (95).

ITC

ITC titrations were performed at 25 or 37 °C using a VP-ITC microcalorimeter (MicroCal/Malvern Instruments). Titrations were conducted in HBS buffer supplemented with 1 mM EGTA or 0.5 mM $CaCl_2$. Samples were degassed for at least 15 min. 5–10 μM CaM was placed in the ITC cell, and 50–200 μM peptide was added to the titration syringe. Each ITC experiment consisted of at least 24 injections of 10 μl of titrant, preceded by one 2-μl injection, which is traditionally used to "prime" the system for ligand diffusion during the temperature equilibration between the syringe and cell contents (96). Data were analyzed with MicroCal Origin version 7.0, using the built-in curve-fitting models.

Crystallization, structure determination, and refinement

WT CaM purified in-house (see above) was mixed with Q4A in an equimolar ratio at room temperature, in HBS buffer supplemented with 2 mM $CaCl_2$ or 2 mM EGTA, and Q4B was added at an equimolar ratio 30 min later. The final concentration of each protein was 222 μM. Automated screening for crystallization was carried out using the sitting drop vapor-diffusion method with an Art Robbins Instruments Phoenix system in the X-ray Crystallography Core Laboratory at UT Health San Antonio. Crystals of Ca^{2+}-loaded complexes were initially obtained from Microlytic MCSG-III screen condition 60; optimized in 1.3 M sodium citrate, 0.1 M HEPES, pH 7.0; and flash-cooled in liquid nitrogen prior to data collection. Data for two crystals were collected at the Advanced Photon Source NE-CAT beamline 24-ID-E and integrated and scaled together using XDS (97). The structure of Ca^{2+}/CaM:Q4A:Q4B was determined by the molecular replacement method implemented in PHASER (98) using a truncated version of PDB entry 4UMO as the search model. Coordinates were refined using PHENIX (99), including simulated annealing with torsion angle dynamics and TLS refinement, alternated with manual rebuilding using COOT (100). The model was verified using composite omit map analysis (101, 102) to minimize model bias. Data collection and refinement statistics are shown in Table S1. Renderings of the structures were performed using PyMOL software (PyMOL Molecular Graphics System, version 2.0, Schrödinger, LLC).

MST

apoCaM in ChHBS was conjugated with Alexa Fluor 594 (Alexa-CaM) using a protein-labeling kit (Invitrogen). Q4B or Q4A peptides were serially diluted 1:2 in ChHBS containing an additional 0.5 mM EGTA. The final concentration of Alexa-CaM in each well of the dilution series was 200 nM, and each sample was centrifuged prior to loading to standard capillaries. After capturing the proteins in 16 different capillaries, fluorescence was measured in a Nanotemper Monolith 1.115, using an excitation power of 60 and MST power of 80. Microscale thermophoresis was recorded using the MO control software, and the binding affinities were analyzed using PALMIST and GUSSI (Chad Brautigam, UT Southwestern, Dallas, TX) (103, 104).

HSQC-NMR

NMR titrations of [^{15}N]CaM with unlabeled Q4A and Q4B peptides were performed using HSQC (non-TROSY) experiments. All non-TROSY experiments were conducted in HBS, 1 mM EGTA, and 10% (v/v) D_2O at 298 K on a Bruker Avance 700 NMR spectrometer. NMR titrations of deuterated [^{2}H-^{15}N]CaM with Ca^{2+} were performed in ChHBS using TROSY-HSQC to reduce line broadening by cancelling dipole–dipole coupling and chemical shift anisotropy, thus producing well-resolved spectra. The methods were performed similarly to those described elsewhere (105, 106).

The assignments for mammalian apoCaM were shared with us by John Putkey (UT Health, Houston, TX), and the assignments for Ca^{2+}/CaM were kindly provided by Walter Chazin (Vanderbilt University, Nashville, TN) and Adriaan Bax (National Institutes of Health, Bethesdsa, MD). The raw spectrometer format data were processed using nmrPipe and nmrDraw (107). The peaks were calculated and visualized using SPARKY version 3.115 software (T. D. Goddard and D. G. Kneller, University of California, San Francisco), and in some cases, the overlays were formatted using Adobe Illustrator.

Estimation of equilibrium constants of apoCaM for the KCNQ4 B domain were evaluated by NMR titration data as follows. The peak heights of the titration spectra were normalized against the reference spectrum without titrant, followed by calculation of the mean and S.D. of the normalized peak heights after titration. Only those residues showing normalized peak heights at least 2 × S.D. above the mean were plotted. Using these peak data, the K_d values were determined using GraphPad Prism version 7, by fitting those data to the binding equation, $y = B_{max} \cdot x/(K_d + x) + NS \cdot x +$ background, in the one-site–total nonlinear model. Although plotting peak height (line broadening) is not a widely accepted or accurate method for determining affinities, we used this method as an approximation to guide us in further experimental approaches for testing binding affinities.

Perforated patch-clamp electrophysiology

CHO cells were grown in 100-mm tissue culture dishes (Falcon, Franklin Lakes, NJ) in Dulbecco's modified Eagle's medium with 10% heat-inactivated fetal bovine serum plus 0.1% penicillin/streptomycin in a humidified incubator at 37 °C (5% CO_2) and passaged every 4 days. Cells were discarded after ~30 passages. CHO cells were first passaged onto 35-mm plastic tissue culture dishes and transfected 24 h later with FuGENE HD reagent (Promega), according to the manufacturer's instructions. The total amount of cDNA used was 0.55 μg, which is less than that typical but required for such high-expressing channels like KCNQ4 (41), which otherwise might "soak-up" all of the PIP_2 in the membrane, allowing artifactual interactions between CaM and the channels that are unphysiological. The next day, cells were plated onto coverglass chips, and experiments were performed over the following 1–2 days. Pipettes were pulled from borosilicate glass capillaries (BF150-86-10HP; Sutter Instruments) using a Flaming/Brown micropipette puller P-97 (Sutter Instruments) and had resistances of 2–3 MΩ when filled with internal solution and measured in

standard bath solution. The external Ringer's solution contained 160 mM NaCl, 5 mM KCl, 2 mM $CaCl_2$, 1 mM $MgCl_2$, and 10 mM HEPES, pH 7.4, with NaOH. The pipette solution contained 160 mM KCl, 5 mM $MgCl_2$, and 10 mM HEPES, pH 7.4, with KOH with added amphotericin B.

Membrane current was measured with pipette and membrane capacitance cancellation, sampled at 5 ms, and filtered at 1 kHz using an EPC10 amplifier and Patchmaster software (HEKA). In all experiments, the perforated patch method of recording was used with amphotericin B (600 ng/ml) in the pipette solution (108). Amphotericin was prepared as a stock solution as 60 mg/ml in DMSO. In these experiments, the access resistance was typically 7–15 MΩ, 5–10 min after seal formation. Series resistance compensation was routinely compensated ~60%, and liquid junction potential corrections (<2 mV in this case) were not applied. Cells were placed in a 500-μl perfusion chamber through which solution flowed at 1–2 ml/min. Inflow to the chamber was by gravity from several reservoirs, selectable by activation of solenoid valves (Warner Scientific). Bath solution exchange was essentially complete by <30 s. Experiments were performed at room temperature. Cells that displayed KCNQ4 currents over 1 nA at 0 mV were not studied, nor were experiments accepted if the uncorrected series resistance was >5 MΩ, due to undue sequestering of free $[PIP_2]$ or to residual series resistance voltage errors. Currents were studied by holding the membrane potential at −80 mV and applying 500-ms depolarizing pulses from −80 to 40 mV, followed by a 400-ms step to −60 mV, every 3 s. To estimate voltage dependence, tail current amplitudes at −60 mV were fit to a single exponential starting at a time ~5–10 ms after the repolarization (when the residual capacity transient has subsided), and the amplitudes were normalized and plotted as a function of test potential. The data were fit with Boltzmann relations of the form, $I/I_{max} = I_{max}/(1 + \exp((V_{½} - V)/k))$, where I_{max} is the maximum tail current, $V_{½}$ is the voltage that produces half-maximal activation of the conductance, and k is the slope factor. Values from cell populations were compared using a two-tailed t test. In such group comparisons, the use of S.E. values is most statistically correct. The activation kinetics were estimated using a weighted double-exponential fit ($A{\cdot}\exp(-\tau/t_1) + B{\cdot}\exp(-\tau/t_2)$) of the first 400 ms of the currents, where τ_1 and τ_2 are the fast and slow time constants and A and B are the "weights." Thus, the weighted deactivation time constants reported are given by $(A{\cdot}\tau_1 + B{\cdot}\tau_2)/(A + B)$. The deactivation time constants were measured by fitting the deactivating current to a single exponential at −60 mV, as described above.

Author contributions—C. R. A., A. B. T., and M. S. S. conceptualization; C. R. A., A. B. T., V. D. l. R., A. B., and M. S. S. formal analysis; C. R. A. and M. S. S. funding acquisition; C. R. A., B. T. E., A. B. T., A. B., and M. S. S. validation; C. R. A., B. T. E., A. B. T., V. D. l. R., A. B., and M. S. S. investigation; C. R. A., A. B. T., V. D. l. R., and A. B. visualization; C. R. A., B. T. E., A. B. T., and V. D. l. R. writing-original draft; C. R. A., A. B., and M. S. S. writing-review and editing; B. T. E., A. B. T., A. B., and M. S. S. data curation; B. T. E., A. B. T., A. B., and M. S. S. methodology; A. B. T., A. B., and M. S. S. resources; A. B. T. and A. B. software; M. S. S. supervision and project administration.

Acknowledgments—We thank Yinghua Chen (Case Western Reserve University, Cleveland, OH) for preparing the Alexa Fluor 594 proteins and providing expertise in MST analysis and Pamela Reed, MaryAnn Hobbs, and Isamar Sanchez for expert technical support. We are indebted to the following facilities of the Institutional Research Cores at UT Health San Antonio in the Department of Biochemistry: the Center for Macromolecular Interactions, directed by Drs. Eileen Lafer and Bo Demeler; the X-ray Crystallography Core Laboratory, directed by Drs. P. John Hart and Alex Taylor; and the NMR spectroscopy core, directed by Dr. Dmitri Ivanov. Institutional Research Cores at UT Health San Antonio are supported by the Office of the Vice President for Research and the Mays Cancer Center, the center home to the UT Health San Antonio MD Anderson Cancer Center (National Institutes of Health Grant P30 CA054174). We also gratefully thank Drs. Eileen Lafer, Bo Demeler, and Dmitri Ivanov (Department of Biochemistry and Structural Biology), Robert Brenner (Department of Cell and Integrative Physiology), Brad Rothberg (Temple University), Chad Brautigam (UT Southwestern), Sudha Chakrapani (Case Western Reserve University), and William N. Zagotta (University of Washington) for many helpful discussions regarding this project. We are further indebted to James D. Stockand for providing the necessary time for C. R. A. to finish the manuscript.

References

1. Faas, G. C., Raghavachari, S., Lisman, J. E., and Mody, I. (2011) Calmodulin as a direct detector of Ca^{2+} signals. *Nat. Neurosci.* **14,** 301–304 CrossRef Medline
2. Westerlund, A. M., and Delemotte, L. (2018) Effect of Ca^{2+} on the promiscuous target-protein binding of calmodulin. *PLoS Comput. Biol.* **14,** e1006072 CrossRef Medline
3. Tjandra, N., Kuboniwa, H., Ren, H., and Bax, A. (1995) Rotational dynamics of calcium-free calmodulin studied by ^{15}N-NMR relaxation measurements. *Eur. J. Biochem.* **230,** 1014–1024 CrossRef Medline
4. Linse, S., Helmersson, A., and Forsén, S. (1991) Calcium binding to calmodulin and its globular domains. *J. Biol. Chem.* **266,** 8050–8054 Medline
5. Zhang, M., Tanaka, T., and Ikura, M. (1995) Calcium-induced conformational transition revealed by the solution structure of apo calmodulin. *Nat. Struct. Biol.* **2,** 758–767 CrossRef Medline
6. Zhang, P., Tripathi, S., Trinh, H., and Cheung, M. S. (2017) Opposing intermolecular tuning of Ca^{2+} affinity for calmodulin by neurogranin and CaMKII peptides. *Biophys. J.* **112,** 1105–1119 CrossRef Medline
7. Gamper, N., and Shapiro, M. S. (2003) Calmodulin mediates Ca^{2+}-dependent modulation of M-type K^+ channels. *J. Gen. Physiol.* **122,** 17–31 CrossRef Medline
8. Beech, D. J., Bernheim, L., Mathie, A., and Hille, B. (1991) Intracellular Ca^{2+} buffers disrupt muscarinic suppression of Ca^{2+} current and M current in rat sympathetic neurons. *Proc. Natl. Acad. Sci. U.S.A.* **88,** 652–656 CrossRef Medline
9. Neher, E. (1998) Vesicle pools and Ca^{2+} microdomains: new tools for understanding their roles in neurotransmitter release. *Neuron* **20,** 389–399 CrossRef Medline
10. Crivici, A., and Ikura, M. (1995) Molecular and structural basis of target recognition by calmodulin. *Annu. Rev. Biophys. Biomol. Struct.* **24,** 85–116 CrossRef Medline
11. Geiser, J. R., van Tuinen, D., Brockerhoff, S. E., Neff, M. M., and Davis, T. N. (1991) Can calmodulin function without binding calcium? *Cell* **65,** 949–959 CrossRef Medline
12. Keen, J. E., Khawaled, R., Farrens, D. L., Neelands, T., Rivard, A., Bond, C. T., Janowsky, A., Fakler, B., Adelman, J. P., and Maylie, J. (1999) Domains responsible for constitutive and Ca^{2+}-dependent interactions between calmodulin and small conductance Ca^{2+}-activated potassium channels. *J. Neurosci.* **19,** 8830–8838 CrossRef Medline

13. Peterson, B. Z., DeMaria, C. D., Adelman, J. P., and Yue, D. T. (1999) Calmodulin is the Ca^{2+} sensor for Ca^{2+} -dependent inactivation of L-type calcium channels. *Neuron* **22,** 549–558 CrossRef Medline
14. Zühlke, R. D., Pitt, G. S., Tsien, R. W., and Reuter, H. (2000) Ca^{2+}-sensitive inactivation and facilitation of L-type Ca^{2+} channels both depend on specific amino acid residues in a consensus calmodulin-binding motif in the $\alpha 1_C$ subunit. *J. Biol. Chem.* **275,** 21121–21129 CrossRef Medline
15. Clapham, D. E. (2007) Calcium signaling. *Cell* **131,** 1047–1058 CrossRef Medline
16. Ben-Johny, M., and Yue, D. T. (2014) Calmodulin regulation (calmodulation) of voltage-gated calcium channels. *J. Gen. Physiol.* **143,** 679–692 CrossRef Medline
17. DeMaria, C. D., Soong, T. W., Alseikhan, B. A., Alvania, R. S., and Yue, D. T. (2001) Calmodulin bifurcates the local Ca^{2+} signal that modulates P/Q-type Ca^{2+} channels. *Nature* **411,** 484–489 CrossRef Medline
18. Erickson, M. G., Alseikhan, B. A., Peterson, B. Z., and Yue, D. T. (2001) Preassociation of calmodulin with voltage-gated Ca^{2+} channels revealed by FRET in single living cells. *Neuron* **31,** 973–985 CrossRef Medline
19. Halling, D. B., Aracena-Parks, P., and Hamilton, S. L. (2006) Regulation of voltage-gated Ca^{2+} channels by calmodulin. *Sci. STKE* **2006,** er1 Medline
20. Lee, A., Scheuer, T., and Catterall, W. A. (2000) Ca^{2+}/calmodulin-dependent facilitation and inactivation of P/Q-type Ca^{2+} channels. *J. Neurosci.* **20,** 6830–6838 CrossRef Medline
21. Liang, H., DeMaria, C. D., Erickson, M. G., Mori, M. X., Alseikhan, B. A., and Yue, D. T. (2003) Unified mechanisms of Ca^{2+} regulation across the Ca^{2+} channel family. *Neuron* **39,** 951–960 CrossRef Medline
22. Zamponi, G. W. (2003) Calmodulin lobotomized: novel insights into calcium regulation of voltage-gated calcium channels. *Neuron* **39,** 879–881 CrossRef Medline
23. Xia, X. M., Fakler, B., Rivard, A., Wayman, G., Johnson-Pais, T., Keen, J. E., Ishii, T., Hirschberg, B., Bond, C. T., Lutsenko, S., Maylie, J., and Adelman, J. P. (1998) Mechanism of calcium gating in small-conductance calcium-activated potassium channels. *Nature* **395,** 503–507 CrossRef Medline
24. Schumacher, M. A., Rivard, A. F., Bächinger, H. P., and Adelman, J. P. (2001) Structure of the gating domain of a Ca^{2+}-activated K^+ channel complexed with Ca^{2+}/calmodulin. *Nature* **410,** 1120–1124 CrossRef Medline
25. Maylie, J., Bond, C. T., Herson, P. S., Lee, W. S., and Adelman, J. P. (2004) Small conductance Ca^{2+}-activated K^+ channels and calmodulin. *J. Physiol.* **554,** 255–261 CrossRef Medline
26. Lee, C. H., and MacKinnon, R. (2018) Activation mechanism of a human SK-calmodulin channel complex elucidated by cryo-EM structures. *Science* **360,** 508–513 CrossRef Medline
27. Gamper, N., and Shapiro, M. S. (2015) KCNQ Channels. in *Handbook of Ion Channels* (Zheng, J., and Trudeau, M., eds) CRC Press, Boca Raton, FL
28. Etxeberria, A., Aivar, P., Rodriguez-Alfaro, J. A., Alaimo, A., Villacé, P., Gómez-Posada, J. C., Areso, P., and Villarroel, A. (2008) Calmodulin regulates the trafficking of KCNQ2 potassium channels. *FASEB J.* **22,** 1135–1143 CrossRef Medline
29. Gao, Y., Yechikov, S., Vázquez, A. E., Chen, D., and Nie, L. (2013) Impaired surface expression and conductance of the KCNQ4 channel lead to sensorineural hearing loss. *J. Cell Mol. Med.* **17,** 889–900 CrossRef Medline
30. Kosenko, A., and Hoshi, N. (2013) A change in configuration of the calmodulin-KCNQ channel complex underlies Ca^{2+}-dependent modulation of KCNQ channel activity. *PLoS One* **8,** e82290 CrossRef Medline
31. Liu, W., and Devaux, J. J. (2014) Calmodulin orchestrates the heteromeric assembly and the trafficking of KCNQ2/3 (Kv7.2/3) channels in neurons. *Mol. Cell Neurosci.* **58,** 40–52 CrossRef Medline
32. Zaika, O., Zhang, J., and Shapiro, M. S. (2011) Combined phosphoinositide and Ca^{2+} signals mediating receptor specificity toward neuronal Ca^{2+} channels. *J. Biol. Chem.* **286,** 830–841 CrossRef Medline
33. Tobelaim, W. S., Dvir, M., Lebel, G., Cui, M., Buki, T., Peretz, A., Marom, M., Haitin, Y., Logothetis, D. E., Hirsch, J. A., and Attali, B. (2017) Competition of calcified calmodulin N lobe and PIP_2 to an LQT mutation site in Kv7.1 channel. *Proc. Natl. Acad. Sci. U.S.A.* **114,** E869–E878 CrossRef Medline
34. Shamgar, L., Ma, L., Schmitt, N., Haitin, Y., Peretz, A., Wiener, R., Hirsch, J., Pongs, O., and Attali, B. (2006) Calmodulin is essential for cardiac IKS channel gating and assembly: impaired function in long-QT mutations. *Circ. Res.* **98,** 1055–1063 CrossRef Medline
35. Peroz, D., Rodriguez, N., Choveau, F., Baró, I., Mérot, J., and Loussouarn, G. (2008) Kv7.1 (KCNQ1) properties and channelopathies. *J. Physiol.* **586,** 1785–1789 CrossRef Medline
36. Rocheleau, J. M., and Kobertz, W. R. (2008) KCNE peptides differently affect voltage sensor equilibrium and equilibration rates in KCNQ1 K^+ channels. *J. Gen. Physiol.* **131,** 59–68 CrossRef Medline
37. Alaimo, A., Gómez-Posada, J. C., Aivar, P., Etxeberría, A., Rodriguez-Alfaro, J. A., Areso, P., and Villarroel, A. (2009) Calmodulin activation limits the rate of KCNQ2 K^+ channel exit from the endoplasmic reticulum. *J. Biol. Chem.* **284,** 20668–20675 CrossRef Medline
38. Haitin, Y., and Attali, B. (2008) The C-terminus of Kv7 channels: a multifunctional module. *J. Physiol.* **586,** 1803–1810 CrossRef Medline
39. Wen, H., and Levitan, I. B. (2002) Calmodulin is an auxiliary subunit of KCNQ2/3 potassium channels. *J. Neurosci.* **22,** 7991–8001 CrossRef Medline
40. Yus-Najera, E., Santana-Castro, I., and Villarroel, A. (2002) The identification and characterization of a noncontinuous calmodulin-binding site in noninactivating voltage-dependent KCNQ potassium channels. *J. Biol. Chem.* **277,** 28545–28553 CrossRef Medline
41. Hernandez, C. C., Zaika, O., and Shapiro, M. S. (2008) A carboxy-terminal inter-helix linker as the site of phosphatidylinositol 4,5-bisphosphate action on Kv7 (M-type) K^+ channels. *J. Gen. Physiol.* **132,** 361–381 CrossRef Medline
42. Higashida, H., Hoshi, N., Zhang, J. S., Yokoyama, S., Hashii, M., Jin, D., Noda, M., and Robbins, J. (2005) Protein kinase C bound with A-kinase anchoring protein is involved in muscarinic receptor-activated modulation of M-type KCNQ potassium channels. *Neurosci. Res.* **51,** 231–234 CrossRef Medline
43. Hoshi, N., Zhang, J. S., Omaki, M., Takeuchi, T., Yokoyama, S., Wanaverbecq, N., Langeberg, L. K., Yoneda, Y., Scott, J. D., Brown, D. A., and Higashida, H. (2003) AKaP150 signaling complex promotes suppression of the M current by muscarinic agonists. *Nat. Neurosci.* **6,** 564–571 CrossRef Medline
44. Kosenko, A., Kang, S., Smith, I. M., Greene, D. L., Langeberg, L. K., Scott, J. D., and Hoshi, N. (2012) Coordinated signal integration at the M-type potassium channel upon muscarinic stimulation. *EMBO J.* **31,** 3147–3156 CrossRef Medline
45. Strulovich, R., Tobelaim, W. S., Attali, B., and Hirsch, J. A. (2016) Structural insights into the M channel proximal C-terminus/calmodulin complex. *Biochemistry* **55,** 5353–5365 CrossRef Medline
46. Sachyani, D., Dvir, M., Strulovich, R., Tria, G., Tobelaim, W., Peretz, A., Pongs, O., Svergun, D., Attali, B., and Hirsch, J. A. (2014) Structural basis of a Kv7.1 potassium channel gating module: studies of the intracellular C-terminal domain in complex with calmodulin. *Structure* **22,** 1582–1594 CrossRef Medline
47. Sun, J., and MacKinnon, R. (2017) Cryo-EM Structure of a KCNQ1/CaM complex reveals insights into congenital long-QT syndrome. *Cell* **169,** 1042–1050.e9 CrossRef Medline
48. Chang, A., Abderemane-Ali, F., Hura, G. L., Rossen, N. D., Gate, R. E., and Minor, D. L., Jr. (2018) A calmodulin C-lobe Ca^{2+}-dependent switch governs Kv7 channel function. *Neuron* **97,** 836–852.e6 CrossRef Medline
49. Xu, Q., Chang, A., Tolia, A., and Minor, D. L., Jr. (2013) Structure of a Ca^{2+}/CaM:Kv7.4 (KCNQ4) B-helix complex provides insight into M-current modulation. *J. Mol. Biol.* **425,** 378–394 CrossRef Medline
50. Bernardo-Seisdedos, G., Nuñez, E., Gomis-Perez, C., Malo, C., Villarroel, Á., and Millet, O. (2018) Structural basis and energy landscape for the Ca^{2+} gating and calmodulation of the Kv7.2 K^+ channel. *Proc. Natl. Acad. Sci. U.S.A.* **115,** 2395–2400 CrossRef Medline
51. Houdusse, A., Silver, M., and Cohen, C. (1996) A model of Ca^{2+}-free calmodulin binding to unconventional myosins reveals how calmodulin acts as a regulatory switch. *Structure* **4,** 1475–1490 CrossRef Medline

52. Mruk, K., Farley, B. M., Ritacco, A. W., and Kobertz, W. R. (2014) Calmodulation meta-analysis: predicting calmodulin binding via canonical motif clustering. *J. Gen. Physiol.* **144,** 105–114 CrossRef Medline
53. Liu, Z., and Vogel, H. J. (2012) Structural basis for the regulation of L-type voltage-gated calcium channels: interactions between the N-terminal cytoplasmic domain and Ca^{2+}-calmodulin. *Front. Mol. Neurosci.* **5,** 38 CrossRef Medline
54. Evans, T. I., Hell, J. W., and Shea, M. A. (2011) Thermodynamic linkage between calmodulin domains binding calcium and contiguous sites in the C-terminal tail of $Ca_V1.2$. *Biophys. Chem.* **159,** 172–187 CrossRef Medline
55. Keowmaneechai, E., and McClements, D. J. (2002) Influence of EDTA and citrate on physicochemical properties of whey protein-stabilized oil-in-water emulsions containing $CaCl_2$. *J. Agric. Food Chem.* **50,** 7145–7153 CrossRef Medline
56. Neufeld, T., Eisenstein, M., Muszkat, K. A., and Fleminger, G. (1998) A citrate-binding site in calmodulin. *J. Mol. Recognit.* **11,** 20–24 CrossRef Medline
57. Gamper, N., Li, Y., and Shapiro, M. S. (2005) Structural requirements for differential sensitivity of KCNQ K^+ channels to modulation by Ca^{2+}/calmodulin. *Mol. Biol. Cell* **16,** 3538–3551 CrossRef Medline
58. Alaimo, A., Alberdi, A., Gomis-Perez, C., Fernández-Orth, J., Gómez-Posada, J. C., Areso, P., and Villarroel, A. (2013) Cooperativity between calmodulin-binding sites in Kv7.2 channels. *J. Cell Sci.* **126,** 244–253 CrossRef Medline
59. Xu, T., Nie, L., Zhang, Y., Mo, J., Feng, W., Wei, D., Petrov, E., Calisto, L. E., Kachar, B., Beisel, K. W., Vazquez, A. E., and Yamoah, E. N. (2007) Roles of alternative splicing in the functional properties of inner ear-specific KCNQ4 channels. *J. Biol. Chem.* **282,** 23899–23909 CrossRef Medline
60. Shahidullah, M., Santarelli, L. C., Wen, H., and Levitan, I. B. (2005) Expression of a calmodulin-binding KCNQ2 potassium channel fragment modulates neuronal M-current and membrane excitability. *Proc. Natl. Acad. Sci. U.S.A.* **102,** 16454–16459 CrossRef Medline
61. Hernandez, C. C., Zaika, O., Tolstykh, G. P., and Shapiro, M. S. (2008) Regulation of neural KCNQ channels: signalling pathways, structural motifs and functional implications. *J. Physiol.* **586,** 1811–1821 CrossRef Medline
62. Etzioni, A., Siloni, S., Chikvashvilli, D., Strulovich, R., Sachyani, D., Regev, N., Greitzer-Antes, D., Hirsch, J. A., and Lotan, I. (2011) Regulation of neuronal M-channel gating in an isoform-specific manner: functional interplay between calmodulin and syntaxin 1A. *J. Neurosci.* **31,** 14158–14171 CrossRef Medline
63. Gamper, N., Zaika, O., Li, Y., Martin, P., Hernandez, C. C., Perez, M. R., Wang, A. Y., Jaffe, D. B., and Shapiro, M. S. (2006) Oxidative modification of M-type K^+ channels as a mechanism of cytoprotective neuronal silencing. *EMBO J.* **25,** 4996–5004 CrossRef Medline
64. Linley, J. E., Ooi, L., Pettinger, L., Kirton, H., Boyle, J. P., Peers, C., and Gamper, N. (2012) Reactive oxygen species are second messengers of neurokinin signaling in peripheral sensory neurons. *Proc. Natl. Acad. Sci. U.S.A.* **109,** E1578–E1586 CrossRef Medline
65. Ooi, L., Gigout, S., Pettinger, L., and Gamper, N. (2013) Triple cysteine module within M-type K^+ channels mediates reciprocal channel modulation by nitric oxide and reactive oxygen species. *J. Neurosci.* **33,** 6041–6046 CrossRef Medline
66. Wang, Q., Zhang, P., Hoffman, L., Tripathi, S., Homouz, D., Liu, Y., Waxham, M. N., and Cheung, M. S. (2013) Protein recognition and selection through conformational and mutually induced fit. *Proc. Natl. Acad. Sci. U.S.A.* **110,** 20545–20550 CrossRef Medline
67. Wang, C., Chung, B. C., Yan, H., Wang, H. G., Lee, S. Y., and Pitt, G. S. (2014) Structural analyses of Ca^{2+}/CaM interaction with NaV channel C-termini reveal mechanisms of calcium-dependent regulation. *Nat. Commun.* **5,** 4896 CrossRef Medline
68. Gabelli, S. B., Boto, A., Kuhns, V. H., Bianchet, M. A., Farinelli, F., Aripirala, S., Yoder, J., Jakoncic, J., Tomaselli, G. F., and Amzel, L. M. (2014) Regulation of the $Na_V1.5$ cytoplasmic domain by calmodulin. *Nat. Commun.* **5,** 5126 CrossRef Medline
69. Falkenburger, B. H., Jensen, J. B., Dickson, E. J., Suh, B. C., and Hille, B. (2010) Phosphoinositides: lipid regulators of membrane proteins. *J. Physiol.* **588,** 3179–3185 CrossRef Medline
70. Suh, B. C., and Hille, B. (2007) Regulation of KCNQ channels by manipulation of phosphoinositides. *J. Physiol.* **582,** 911–916 CrossRef Medline
71. Zaydman, M. A., Silva, J. R., Delaloye, K., Li, Y., Liang, H., Larsson, H. P., Shi, J., and Cui, J. (2013) Kv7.1 ion channels require a lipid to couple voltage sensing to pore opening. *Proc. Natl. Acad. Sci. U.S.A.* **110,** 13180–13185 CrossRef Medline
72. Cui, Y., Wen, J., Hung Sze, K., Man, D., Lin, D., Liu, M., and Zhu, G. (2003) Interaction between calcium-free calmodulin and IQ motif of neurogranin studied by nuclear magnetic resonance spectroscopy. *Anal. Biochem.* **315,** 175–182 CrossRef Medline
73. Kaleka, K. S., Petersen, A. N., Florence, M. A., and Gerges, N. Z. (2012) Pull-down of calmodulin-binding proteins. *J. Vis. Exp.* 10.3791/3502 CrossRef Medline
74. Kubota, Y., Putkey, J. A., and Waxham, M. N. (2007) Neurogranin controls the spatiotemporal pattern of postsynaptic Ca^{2+}/CaM signaling. *Biophys. J.* **93,** 3848–3859 CrossRef Medline
75. Black, D. J., and Persechini, A. (2011) In calmodulin-IQ domain complexes, the Ca^{2+}-free and Ca^{2+}-bound forms of the calmodulin C-lobe direct the N-lobe to different binding sites. *Biochemistry* **50,** 10061–10068 CrossRef Medline
76. Black, D. J., Tran, Q. K., and Persechini, A. (2004) Monitoring the total available calmodulin concentration in intact cells over the physiological range in free Ca^{2+}. *Cell Calcium* **35,** 415–425 CrossRef Medline
77. Tran, Q. K., Black, D. J., and Persechini, A. (2003) Intracellular coupling via limiting calmodulin. *J. Biol. Chem.* **278,** 24247–24250 CrossRef Medline
78. Klingauf, J., and Neher, E. (1997) Modeling buffered Ca^{2+} diffusion near the membrane: implications for secretion in neuroendocrine cells. *Biophys. J.* **72,** 674–690 CrossRef Medline
79. Mori, M. X., Erickson, M. G., and Yue, D. T. (2004) Functional stoichiometry and local enrichment of calmodulin interacting with Ca^{2+} channels. *Science* **304,** 432–435 CrossRef Medline
80. Zhang, J., Carver, C. M., Choveau, F. S., and Shapiro, M. S. (2016) Clustering and functional coupling of diverse ion channels and signaling proteins revealed by super-resolution STORM microscopy in neurons. *Neuron* **92,** 461–478 CrossRef Medline
81. Li, B., Tadross, M. R., and Tsien, R. W. (2016) Sequential ionic and conformational signaling by calcium channels drives neuronal gene expression. *Science* **351,** 863–867 CrossRef Medline
82. Dixon, R. E., Yuan, C., Cheng, E. P., Navedo, M. F., and Santana, L. F. (2012) Ca^{2+} signaling amplification by oligomerization of L-type $Ca_V1.2$ channels. *Proc. Natl. Acad. Sci. U.S.A.* **109,** 1749–1754 CrossRef Medline
83. Vivas, O., Moreno, C. M., Santana, L. F., and Hille, B. (2017) Proximal clustering between BK and $Ca_V1.3$ channels promotes functional coupling and BK channel activation at low voltage. *Elife* **6,** e28029 CrossRef Medline
84. Dick, I. E., Tadross, M. R., Liang, H., Tay, L. H., Yang, W., and Yue, D. T. (2008) A modular switch for spatial Ca^{2+} selectivity in the calmodulin regulation of CaV channels. *Nature* **451,** 830–834 CrossRef Medline
85. Ben Johny, M., Yang, P. S., Bazzazi, H., and Yue, D. T. (2013) Dynamic switching of calmodulin interactions underlies Ca^{2+} regulation of $Ca_V1.3$ channels. *Nat. Commun.* **4,** 1717 CrossRef Medline
86. Ben-Johny, M., Yang, P. S., Niu, J., Yang, W., Joshi-Mukherjee, R., and Yue, D. T. (2014) Conservation of Ca^{2+}/calmodulin regulation across Na and Ca^{2+} channels. *Cell* **157,** 1657–1670 CrossRef Medline
87. Siloni, S., Singer-Lahat, D., Esa, M., Tsemakhovich, V., Chikvashvili, D., and Lotan, I. (2015) Regulation of the neuronal KCNQ2 channel by Src–a dual rearrangement of the cytosolic termini underlies bidirectional regulation of gating. *J. Cell Sci.* **128,** 3489–3501 CrossRef Medline
88. Grabarek, Z. (2011) Insights into modulation of calcium signaling by magnesium in calmodulin, troponin C and related EF-hand proteins. *Biochim. Biophys. Acta* **1813,** 913–921 CrossRef Medline
89. Senguen, F. T., and Grabarek, Z. (2012) X-ray structures of magnesium and manganese complexes with the N-terminal domain of calmodulin: insights into the mechanism and specificity of metal ion binding to an EF-hand. *Biochemistry* **51,** 6182–6194 CrossRef Medline

90. Malmendal, A., Linse, S., Evenäs, J., Forsén, S., and Drakenberg, T. (1999) Battle for the EF-hands: magnesium-calcium interference in calmodulin. *Biochemistry* **38,** 11844–11850 CrossRef Medline
91. Gabelli, S. B., Yoder, J. B., Tomaselli, G. F., and Amzel, L. M. (2016) Calmodulin and Ca^{2+} control of voltage gated Na^+ channels. *Channels* (*Austin*) **10,** 45–54 CrossRef Medline
92. Sutton, R. B., Ernst, J. A., and Brunger, A. T. (1999) Crystal structure of the cytosolic C2A-C2B domains of synaptotagmin III: implications for Ca^{2+}-independent snare complex interaction. *J. Cell Biol.* **147,** 589–598 CrossRef Medline
93. Zhou, Q., Lai, Y., Bacaj, T., Zhao, M., Lyubimov, A. Y., Uervirojnangkoorn, M., Zeldin, O. B., Brewster, A. S., Sauter, N. K., Cohen, A. E., Soltis, S. M., Alonso-Mori, R., Chollet, M., Lemke, H. T., Pfuetzner, R. A., *et al.* (2015) Architecture of the synaptotagmin-SNARE machinery for neuronal exocytosis. *Nature* **525,** 62–67 CrossRef Medline
94. Choveau, F. S., De la Rosa, V., Bierbower, S. M., Hernandez, C. C., and Shapiro, M. S. (2018) Phosphatidylinositol 4,5-bisphosphate (PIP_2) regulates KCNQ3 K^+ channels through multiple sites of action. *J. Biol. Chem.* **293,** 19411–19428 CrossRef Medline
95. Wiedemann, C., Bellstedt, P., and Görlach, M. (2013) CAPITO–a web server-based analysis and plotting tool for circular dichroism data. *Bioinformatics* **29,** 1750–1757 CrossRef Medline
96. Dutta, A. K., Rösgen, J., and Rajarathnam, K. (2015) Erratum: using isothermal titration calorimetry to determine thermodynamic parameters of protein-glycosaminoglycan interactions. *Methods Mol. Biol.* **1229,** E1 CrossRef Medline
97. Kabsch, W. (2010) XDS. *Acta Crystallogr. D Biol. Crystallogr.* **66,** 125–132 CrossRef Medline
98. McCoy, A. J., Grosse-Kunstleve, R. W., Adams, P. D., Winn, M. D., Storoni, L. C., and Read, R. J. (2007) Phaser crystallographic software. *J. Appl. Crystallogr.* **40,** 658–674 CrossRef Medline
99. Adams, P. D., Afonine, P. V., Bunkóczi, G., Chen, V. B., Davis, I. W., Echols, N., Headd, J. J., Hung, L. W., Kapral, G. J., Grosse-Kunstleve, R. W., McCoy, A. J., Moriarty, N. W., Oeffner, R., Read, R. J., Richardson, D. C., *et al.* (2010) PHENIX: a comprehensive Python-based system for macromolecular structure solution. *Acta Crystallogr. D Biol. Crystallogr.* **66,** 213–221 CrossRef Medline
100. Emsley, P., Lohkamp, B., Scott, W. G., and Cowtan, K. (2010) Features and development of Coot. *Acta Crystallogr. D Biol. Crystallogr.* **66,** 486–501 CrossRef Medline
101. Afonine, P. V., Grosse-Kunstleve, R. W., Echols, N., Headd, J. J., Moriarty, N. W., Mustyakimov, M., Terwilliger, T. C., Urzhumtsev, A., Zwart, P. H., and Adams, P. D. (2012) Towards automated crystallographic structure refinement with phenix.refine. *Acta Crystallogr. D Biol. Crystallogr.* **68,** 352–367 CrossRef Medline
102. Terwilliger, T. C., Grosse-Kunstleve, R. W., Afonine, P. V., Moriarty, N. W., Adams, P. D., Read, R. J., Zwart, P. H., and Hung, L. W. (2008) Iterative-build OMIT maps: map improvement by iterative model building and refinement without model bias. *Acta Crystallogr. D Biol. Crystallogr.* **64,** 515–524 CrossRef Medline
103. Brautigam, C. A. (2015) Calculations and publication-quality illustrations for analytical ultracentrifugation data. *Methods Enzymol.* **562,** 109–133 CrossRef Medline
104. Scheuermann, T. H., Padrick, S. B., Gardner, K. H., and Brautigam, C. A. (2016) On the acquisition and analysis of microscale thermophoresis data. *Anal. Biochem.* **496,** 79–93 CrossRef Medline
105. Pervushin, K., Riek, R., Wider, G., and Wüthrich, K. (1997) Attenuated T2 relaxation by mutual cancellation of dipole-dipole coupling and chemical shift anisotropy indicates an avenue to NMR structures of very large biological macromolecules in solution. *Proc. Natl. Acad. Sci. U.S.A.* **94,** 12366–12371 CrossRef Medline
106. Biris, N., Tomashevski, A., Bhattacharya, A., Diaz-Griffero, F., and Ivanov, D. N. (2013) Rhesus monkey TRIM5α SPRY domain recognizes multiple epitopes that span several capsid monomers on the surface of the HIV-1 mature viral core. *J. Mol. Biol.* **425,** 5032–5044 CrossRef Medline
107. Delaglio, F., Grzesiek, S., Vuister, G. W., Zhu, G., Pfeifer, J., and Bax, A. (1995) NMRPipe: a multidimensional spectral processing system based on UNIX pipes. *J. Biomol. NMR* **6,** 277–293 Medline
108. Rae, J., Cooper, K., Gates, P., and Watsky, M. (1991) Low access resistance perforated patch recordings using amphotericin B. *J. Neurosci. Methods* **37,** 15–26 CrossRef Medline